Coordination Chemistry Reviews 270–271 (2014) 89–111

Contents lists available at ScienceDirect

Coordination Chemistry Reviews

journal homepage: www.elsevier.com/locate/ccr

Review

Carbon atoms trapped in cages: Metal carbide clusterfullerenes

Peng Jin [a,**], Chengchun Tang [a], Zhongfang Chen [b,*]

[a] School of Material Science and Engineering, Hebei University of Technology, Tianjin 300130, PR China
[b] Department of Chemistry, Institute for Functional Nanomaterials, University of Puerto Rico, San Juan, PR 00931, USA

Contents

ARTICLE INFO

Article history:
Received 15 July 2013
Received in revised form 23 October 2013
Accepted 24 October 2013
Available online 5 November 2013

Keywords:
Fullerenes
Endohedral metallofullerenes
Clusters

ABSTRACT

Metal carbide clusterfullerenes (MCCFs), which trap two carbon atoms together with metal atom(s) inside the fullerene cage, are a novel branch of endohedral metallofullerenes (EMFs). This review presents an exhaustive survey of recent research progress in MCCFs. After a detailed enumeration of the structural establishments of representative MCCFs, their novel structures, intriguing cluster–cage interplays, fascinating properties, and potential applications are highlighted. Moreover, a variety of new MCCF members are suggested for future identification.

* Corresponding author. Tel.: +1 7875526811.
** Corresponding author.
E-mail addresses: china.peng.jin@gmail.com (P. Jin), zhongfangchen@gmail.com (Z. Chen).

0010-8545/$ – see front matter © 2013 Elsevier B.V. All rights reserved.
http://dx.doi.org/10.1016/j.ccr.2013.10.020

1. Introduction

Endohedral metallofullerenes (EMFs) are novel nanomaterials enclosing a variety of metal ions or metal-containing clusters in various fullerene cages [1–3]. In the past two decades, EMFs have attracted widespread attention due to their unique structures and properties that are remarkably different from their parent cages. A ubiquitous feature of EMFs is the existence of substantial charge transfer from the encased species to the outer carbon frameworks. The negatively charged cages exhibit stabilities that are entirely different from those of the neutral cages. Thus, the formation of EMFs has been employed to help stabilize and synthesize many otherwise labile fullerenes that violate the isolated pentagon rule (IPR) [4] or are of large size [5,6]. More significantly, the physical and chemical properties of EMFs can be tuned by changing the encapsulated species, which endows EMFs with many promising applications in photovoltaics, spintronics, biomedicines, and functional materials [1–3].

Since the first experimental detection of LaC_{60} in 1985 [7], EMFs have a history only a few days shorter than the celebrated C_{60} buckyball [8]. EMFs can be classified in terms of the encapsulated species. Two classical types, monometallofullerenes (mono-EMFs) and dimetallofullerenes (di-EMFs), can be distinguished according to the number of the encased metals. The first stable mono-EMF $La@C_{82}$ [9] and di-EMF $La_2@C_{80}$ [10] were both isolated in 1991. Because the formal charge transferred from each metal to the cage is 3 *e*, their electronic configurations can be denoted as $La^{3+}@C_{82}{}^{3-}$ and $(La^{3+})_2@C_{80}{}^{6-}$, respectively. Thereafter, numerous conventional endofullerenes composed of different metals and cage sizes were successfully synthesized, isolated, and characterized. The encaged metals originate from Groups I to IV on periodical table, with lanthanide being the most popular.

In 1999, the first trimetallic nitride template (TNT) $Sc_3N@C_{80}$ was accidentally discovered (due to N_2 leakage into the arc discharge chamber) by Stevenson et al. and announced the birth of a brand-new branch of EMFs: clusterfullerenes [11]. Its production yield is lower than C_{60} and C_{70} and retains the most abundant EMFs thus far. The successful synthesis of $Sc_3N@C_{80}$ drove a new wave of clusterfullerene fever [12]. To date, in addition to the classical metal nitride clusters (M_3N, such as Sc_3N, Y_3N, Er_3N, and Gd_3N), the inner compositions have expanded to metal carbides ($M_{2,3,4}C_2$, e.g., $Sc_2C_2@C_{84}$) [13], hydrogenated metal carbides (Sc_3CH, e.g., $Sc_3CH@C_{80}$) [14], metal nitrogen carbides (Sc_3NC, e.g., $Sc_3NC@C_{80}$) [15], metal oxides ($Sc_{2,4}O_{1,2,3}$, e.g., $Sc_4O_2@C_{80}$) [16], and metal sulfides (Sc_2S, e.g., $Sc_2S@C_{82}$) [17]. These achievements have greatly enriched the EMF family.

During this "new gold rush era", however, many previously assumed classical EMF structures were seriously challenged. The crisis began in 2001 from the breakthrough reassignment of a Sc_2C_{86} isomer, the previously assumed di-EMF $Sc_2@C_{86}$ (I), as the first metal carbide clusterfullerene (MCCF) $Sc_2C_2@C_{84}$ [13]. In this unprecedented molecule, a C_2 pair is "abandoned" by the C_{84} cage carbons from constituting an otherwise C_{86} skeleton and is unusually trapped together with the Sc atoms inside the hollow. Following this prototype, a variety of new members have joined the MCCF community through experimental findings and/or theoretical predictions, including $Sc_2C_2@C_{68}$ [18], $Y_2C_2@C_{68}$ [19], $La_2C_2@C_{68}$ [19], $Sc_2C_2@C_{72}$ [20], $Sc_2C_2@C_{78}$ [21], $Ti_2C_2@C_{78}$ [22–24], $Zr_2C_2@C_{78}$, $Hf_2C_2@C_{78}$ [25], $Sc_2C_2@C_{80}$ [26], $Sc_3C_2@C_{80}$ [27,28], $Sc_4C_2@C_{80}$ [29], $Sc_2C_2@C_{82}$(I, II, III) [30–32], $Y_2C_2@C_{82}$(I, II, III) [33,34], $ErYC_2@C_{82}$ [35], $Er_2C_2@C_{82}$(I, II, III) [36], $Y_2C_2@C_{84}$ [37–39], $Gd_2C_2@C_{84}$ [39], $Sc_2C_2@C_{86}$ [40], $Lu_3C_2@C_{88}$ [41], $Sc_2C_2@C_{90}$ [40], $Y_2C_2@C_{92}$ [37,42], $Gd_2C_2@C_{92}$ [43,44], and $Y_2C_2@C_{100}$ [37]. A number of these MCCFs have been definitively characterized using single-crystal X-ray crystallography (Table 1). Currently, the synthesis and characterization of new MCCFs has become a notably active research area in fullerene chemistry.

Table 1
Complete list of all reported MCCFs.

MCCFs	Single-crystal structure available?
$Sc_2C_2@C_{68}$	No
$Y_2C_2@C_{68}$	No
$La_2C_2@C_{68}$	No
$Sc_2C_2@C_{72}$	Yes
$Sc_2C_2@C_{78}$	No
$Ti_2C_2@C_{78}$	No
$Zr_2C_2@C_{78}$	No
$Hf_2C_2@C_{78}$	No
$Sc_2C_2@C_{80}$	Yes
$Sc_3C_2@C_{80}$	Yes
$Sc_4C_2@C_{80}$	No
$Sc_2C_2@C_{82}$	Yes
$Y_2C_2@C_{82}$	No
$ErYC_2@C_{82}$	No
$Er_2C_2@C_{82}$	No
$Sc_2C_2@C_{84}$	Yes
$Y_2C_2@C_{84}$	No
$Gd_2C_2@C_{84}$	Yes
$Sc_2C_2@C_{86}$	No
$Lu_3C_2@C_{88}$	No
$Sc_2C_2@C_{90}$	No
$Y_2C_2@C_{92}$	No
$Gd_2C_2@C_{92}$	Yes
$Y_2C_2@C_{100}$	No

Recently, comprehensive reviews have been published regarding conventional EMFs and/or clusterfullerenes [3], and there is also a short account of MCCFs [45]. In contrast to these contributions, this review article specifically focuses on the current research progress of MCCFs from both experimental and theoretical aspects. Particularly highlighted are the novel structures and fascinating properties that differ from conventional mono-, di-, and TNT EMFs. The synthesis (DC-arc discharge of a metal source/graphite composite rod) and separation (multi-step high-performance liquid chromatography (HPLC)) methods for MCCFs are not given in detail because they are the same as for traditional EMFs. For the sake of completeness, other single carbon-trapping clusterfullerenes, such as $Sc_3CH@C_{80}$ [14] and $Sc_3NC@C_{80}$ [15], are also covered.

2. Conventional or unconventional? ($M_m@C_{2n+2}$ vs. $M_mC_2@C_{2n}$)

As mentioned above, the story of MCCFs began with the structure characterization of Sc_2C_{86}, which was first detected in a mass spectrum by Shinohara et al. in 1993 [46]. Two isomers were isolated and were believed to adopt a classical di-EMF $Sc_2@C_{86}$ form in their subsequent spectroscopic experiments [47]. This assumption was soon overturned by the ^{13}C NMR spectrum measurement by the same group [13]. For Sc_2C_{86} (I) in CS_2 solution, 12 lines (10 distinct lines of nearly equal intensity, one line with half the intensity, and an additional line with 1/4 the intensity) were observed (Fig. 1a). None of the 19 IPR isomers of C_{86} [48], however, can exhibit this spectral feature. Therefore, an alternative $Sc_2C_2@C_{84}$ formula with a novel Sc_2C_2 metal carbide unit inside an IPR-satisfying D_{2d}(51591)-C_{84} cage [49] was conceived (Fig. 1b). D_{2d}(51591)-C_{84} is also one of the most abundant C_{84} fullerenes. The ^{13}C NMR spectrum was thus rationalized: 11 of the 12 NMR signals (δ = 129.55–148.27 ppm) stemmed from the parent C_{84} cage, whereas the signal at δ = 92 ppm was attributed to the internal Sc_2C_2 moiety (which is actually due to an impurity as identified in a more sophisticated NMR measurement [50] and a density functional theory (DFT) study [51]). This revolutionary

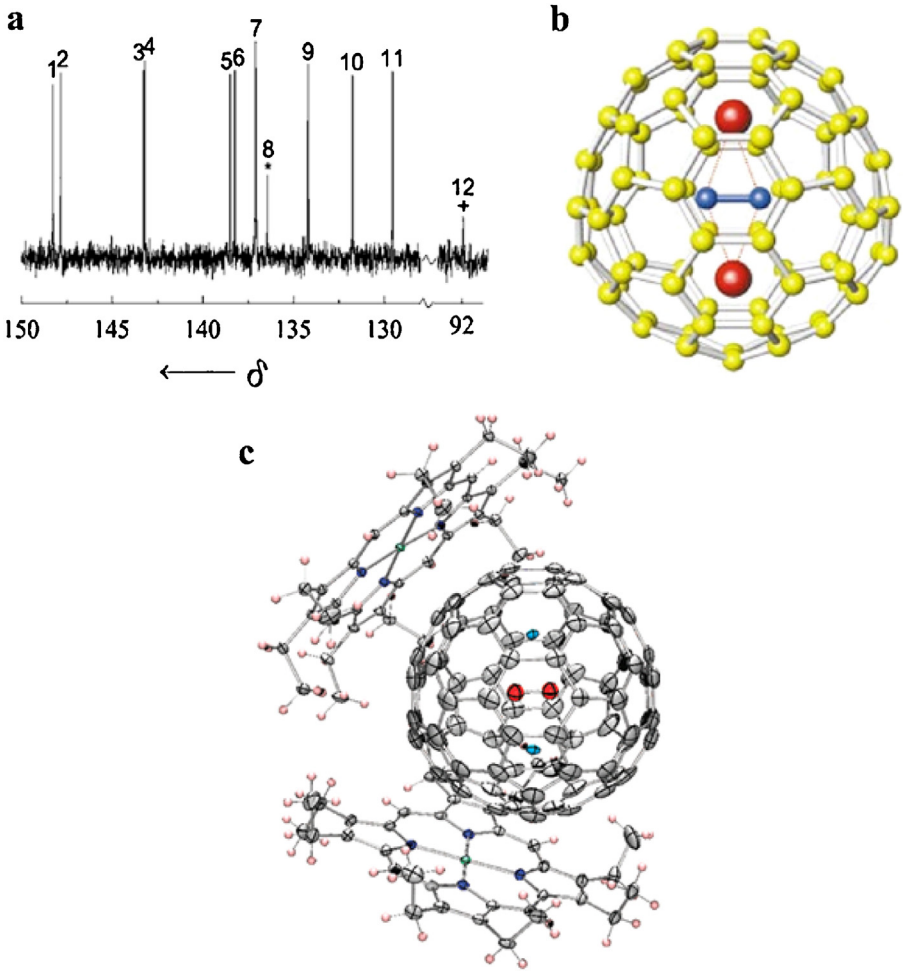

Fig. 1. (a) ^{13}C NMR spectrum of Sc_2C_{86} in CS_2 solution. (b) Schematic representation of the $Sc_2C_2@C_{84}$ molecule. (c) $Sc_2C_2@D_{2d}(51591)$-C_{84}·[Co(OEP)]$_2$·2.5$CHCl_3$·CS_2. Reprinted with permission from Ref. [13]. Copyright Wiley-VCH 2001 (a and b). Reprinted with permission from Ref. [55]. Copyright 2012 American Chemical Society (c).

assignment was further supported by their MEM (maximum entropy method)/Rietveld analysis [52] of synchrotron powder diffraction data. According to the MEM charge density analysis, the formal electronic structure was described as $(Sc_2C_2)^{2+}@C_{84}{}^{2-}$, as a result of a 2 *e* transfer from Sc_2C_2 to C_{84} (further refined as $(Sc^{3+})_2C_2{}^{2-}@C_{84}{}^{4-}$ in Ref. [53]). The encapsulation of Sc_2C_2 into $D_{2d}(51591)$-C_{84} is exothermic (binding energy: ca. 115.0 kcal/mol) according to the DFT calculations [54]. Very recently, the endohedral carbide structure was definitively confirmed by single-crystal X-ray diffraction (XRD) analysis (Fig. 1c) [55].

The discovery of MCCFs is of great significance to EMF characterization. To structurally identify a newly observed metallofullerene, at least two possible candidate formulas should be considered and carefully compared: conventional $M_m@C_{2n+2}$ vs. unconventional $M_mC_2@C_{2n}$. Herein, some representative cases, where MCCFs defeat or coexist with their opponents, are given.

2.1. $Sc_2@C_{70}$ vs. $Sc_2C_2@C_{68}$

Among 8149 cage isomers of C_{70}, only one with D_{5h} symmetry (No. 8149) obeys the IPR [48]. Despite the fact that it is the second most abundant fullerene after C_{60}, no endohedral derivatives of C_{70} were experimentally realized until 1999, when Wang et al. reported the production and isolation of $Sc_2@C_{70}$ [56]. This molecule attracted attention because it was the first structurally confirmed C_{70}-based EMF. Unfortunately, $Sc_2@C_{70}$ was later suggested to actually be a C_{68} cage trapping a Sc_2C_2 cluster inside based on both experimental and theoretical evidence [18,19]. In Shi et al.'s ^{13}C NMR experiment, 21 distinct lines were observed for the Sc_2C_{70} in CS_2 solution (Fig. 2a) [18]. Accordingly, they selectively investigated the possibility of enclosing a Sc_2 dimer in the only IPR $D_{5h}(8149)$-C_{70} cage (Fig. 2b) and all the non-IPR C_{70} isomers featuring 21 nonequivalent carbon types. However, due to the small rotation barrier (1.6 kcal/mol) for the Sc_2 unit, the low energy $Sc_2@D_{5h}(8149)$-C_{70} may exhibit only five NMR lines at room temperature, inconsistent with the 21 lines in the observation. Alternatively, a kinetically more stable $Sc_2C_2@C_{2v}(6073)$-C_{68} isomer satisfies the ^{13}C NMR observation and was finally proposed as the observed species (Fig. 2c). Note that C_{68} has no IPR isomers, and $C_{2v}(6073)$-C_{68} holds two pairs of pentalene motifs. Thus, $Sc_2C_2@C_{68}$ would be not only the first non-IPR MCCF but also the smallest one if unambiguously confirmed. $Y_2C_2@C_{68}$ and $La_2C_2@C_{68}$ were also theoretically investigated [19].

Recently, a conventional $Sc_2@C_{2v}(7854)$-C_{70} structure was suggested to be energetically more stable than $Sc_2C_2@C_{2v}(6073)$-C_{68} by > 30 kcal/mol (with B3LYP and PBE1PBE density functionals), and the simulated UV–vis–NIR spectrum for $Sc_2@C_{2v}(7854)$-C_{70} agrees well with the experimental data [57]. $Sc_2@C_{2v}(7854)$-C_{70} has three pairs of pentagon fusions, two of which are close to the two metal ions (Fig. 2d). Interestingly, $Sc_2C_2@C_{2v}(6073)$-C_{68} and $Sc_2@C_{2v}(7854)$-C_{70} have a similar structural relationship: one can obtain the latter by shifting the carbide carbon atoms of the former outwards to the hexagon ring on the top of the C_{68} cage. Because no concrete single-crystal XRD data are available to date, the debate between $Sc_2@C_{70}$ and $Sc_2C_2@C_{68}$ will surely last for a while.

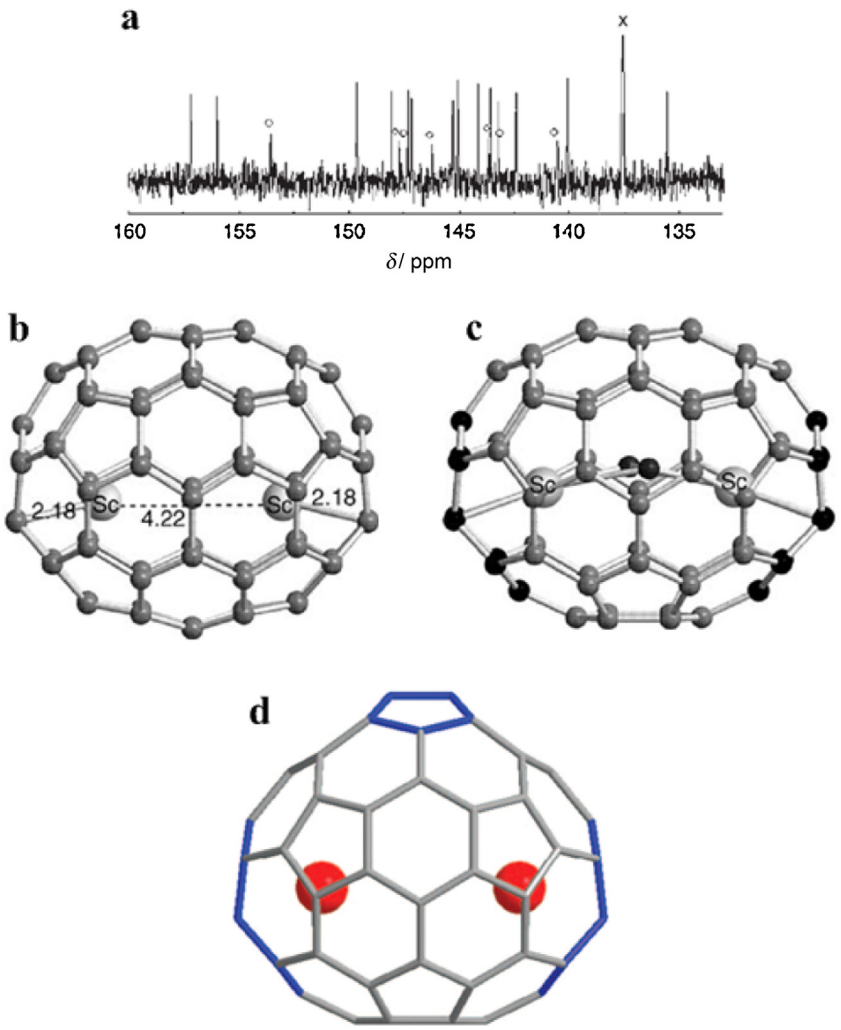

Fig. 2. (a) 125 MHz ^{13}C NMR spectrum of Sc_2C_{70} in CS_2 solution presents 21 lines. Optimized geometry of (b) $Sc_2@D_{5h}(8149)$-C_{70} and (c) $Sc_2C_2@C_{2v}(6073)$-C_{68}. (d) $Sc_2@C_{2v}(7854)$-C_{70} (the adjacent pentagons colored with blue).
Reprinted with permission from Ref. [18]. Copyright Wiley-VCH 2006 (a, b and c). Reprinted with permission from Ref. [57]. Copyright 2012, AIP Publishing LLC (d).

2.2. $Sc_2@C_{74}$ vs. $Sc_2C_2@C_{72}$

Along with Sc_2C_{86}, Sc_2C_{74} was first detected and isolated by Shinohara et al. in 1993 and was proposed as a conventional $Sc_2@C_{74}$ [46]. Without further experimental identification, this molecular formula was adopted for many years (Fig. 3a) [58–63]. Previously, Liu and Hagelberg selectively calculated a $Sc_2C_2@D_{6h}$-C_{72} carbide structure and found that it was energetically much higher than the lowest-energy $Sc_2@C_{74}$ [62]. However, Feng et al. unambiguously characterized Sc_2C_{74} as an MCCF $Sc_2C_2@C_s(10528)$-C_{72} by combining XRD and ^{13}C NMR methods [20]. The single crystal XRD data clearly showed its carbide structure with a $C_s(10528)$-C_{72} outer framework (Fig. 3b). Consistent with the XRD result, they observed 39 lines (33 full, 6 half intensity) in the ^{13}C NMR spectrum. DFT calculations suggested a closed-shell configuration of $(Sc^{3+})_2C_2^{2-}@C_{72}^{4-}$. The $C_s(10528)$-C_{72} is an IPR-violating cage featuring two pairs of fused pentagons. Because the carbide structure of $Sc_2C_2@C_{68}$ is still unjustified [57], $Sc_2C_2@C_s(10528)$-C_{72} is the first experimentally confirmed non-IPR MCCF.

2.3. $Sc_2@C_{80}$ vs. $Sc_2C_2@C_{78}$

In 2004, Wang et al. first isolated three isomers (I, II, III) for Sc_2C_{80} using a three-stage HPLC process [64]. Although the attempt to perform ^{13}C NMR measurements on these three isomers failed, a qualitative comparison of the HPLC retention times (shorter and longer times imply more spherical and more elongated cages, respectively [65]) led them to propose Sc_2C_{80}(I) and Sc_2C_{80}(III) as $Sc_2@I_h(31924)$-C_{80} and $Sc_2@D_{5h}(31923)$-C_{80}, respectively. The detailed structures for the Sc_2C_{80} isomers remained unclear for years until a systematic DFT study was reported in 2012 [21]. According to the computational results, in addition to the two di-EMF isomers, the third isomer is likely $Sc_2C_2@C_{2v}(24107)$-C_{78} due to its favorable energy (Fig. 4). It is a recurrent phenomenon that both conventional and carbide-embedded structures coexist as different isomers of a given EMF [66]. Therefore, relevant structural characterization and identification becomes a highly complicated and challenging task.

2.4. $Ti_2@C_{80}$ vs. $Ti_2C_2@C_{78}$

Ti_2C_{80} was long believed to be a classical di-EMF since its first synthesis by Shinohara's group in 2001 [67–72]. The eight observed lines (3 full, 4 half, and 1 one third intensity; 130–145 ppm) in the ^{13}C NMR spectrum were previously thought to originate from a mixture of two $Ti_2@C_{80}$ isomers bearing D_{5h}- and I_h-C_{80} cages in a ratio of 3:1 (Fig. 5a) [67]. Almost simultaneously in 2005, however, both Yumura et al. [22] and Tan et al. [23] challenged the conventional $Ti_2@C_{80}$ structure with an alternative carbide $Ti_2C_2@C_{78}$ model by means of density functional computations. According to

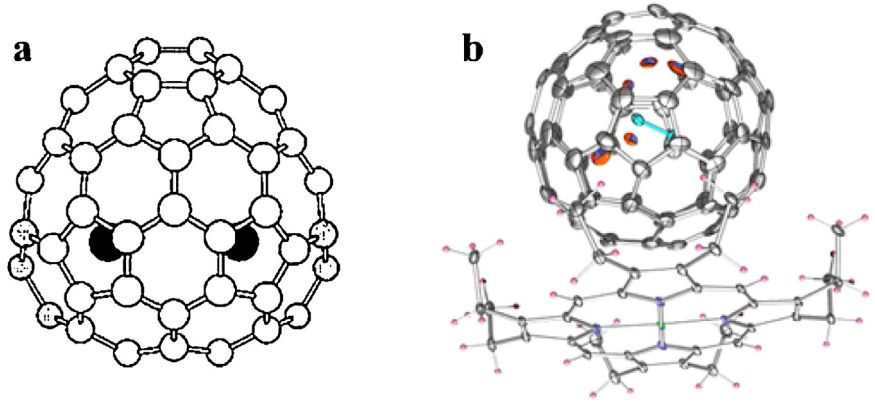

Fig. 3. (a) Optimized structure of $Sc_2@D_{3h}$-C_{74} from Ref. [59]. (b) Ortep drawing of $Sc_2C_2@C_s$(10528)-C_{72}·Ni^{II}(OEP) with 10% thermal ellipsoids. Reproduced from Ref. [20] with permission of The Royal Society of Chemistry.

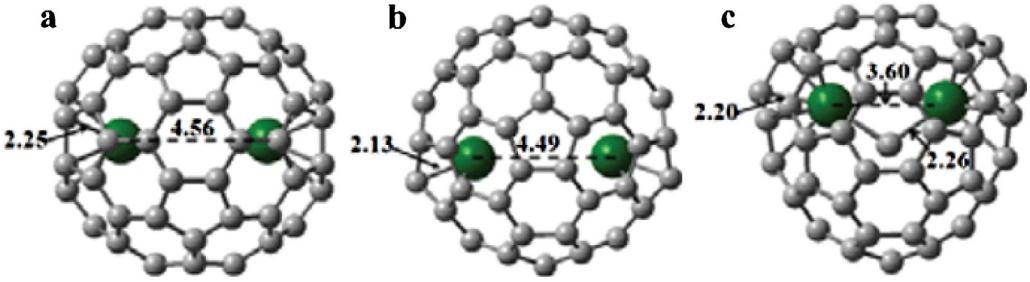

Fig. 4. DFT-optimized structures of (a) $Sc_2@I_h$(31924)-C_{80}, (b) $Sc_2@D_{5h}$(31923)-C_{80} and (c) $Sc_2C_2@C_{2v}$(24107)-C_{78}. Reprinted with permission from Ref. [21]. Copyright Wiley-VCH 2012.

Tan et al.'s computations, the energetically most favorable $Ti_2@I_h$-C_{80} favors a triplet D_{2h} configuration (14.0 kcal/mol lower in energy than its singlet state), thus it should have no signals in the NMR measurement due to its paramagnetic nature. To entrap the Ti_2C_2 cluster, both groups suggested the same D_{3h}(24109)-C_{78} as the most favorable parent cage, which would accept six electrons from the encapsulated metal carbide cluster. The resultant diamagnetic electronic configuration $(Ti^{4+})_2C_2^{2-}@C_{78}^{6-}$ may give rise to eight NMR lines in the typical range for sp^2-hybridized carbon atoms. Yumura et al. found that the encapsulated Ti_2C_2 cluster may adopt either a linear or butterfly configuration (Fig. 5b) depending on the metal binding sites inside the cage, with the former energetically more favorable than the latter. Moreover, the linear isomer is ca. 19.1 kcal/mol lower in energy than the most stable $Ti_2@I_h$-C_{80}. In contrast, a butterfly mode was favored in Tan et al.'s study, in which the C_2 moiety may rotate freely around the C_3 axis of C_{78} with a relatively small energy barrier (ca. 0.1 kcal/mol); thus, the whole molecule essentially exhibits D_{3h} symmetry and eight peaks on the NMR timescale. Recently, the linear-cluster isomer was calibrated as the ground state for $Ti_2C_2@C_{78}$ [25,73]. The simulated chemical shifts for $Ti_2C_2@C_{78}$ are in good agreement with the experiments [23]. Direct experimental evidence for the $Ti_2C_2@C_{78}$ structure was soon reported by Sato et al. [24]. Consistent with the above DFT results, the high-resolution transmission electron

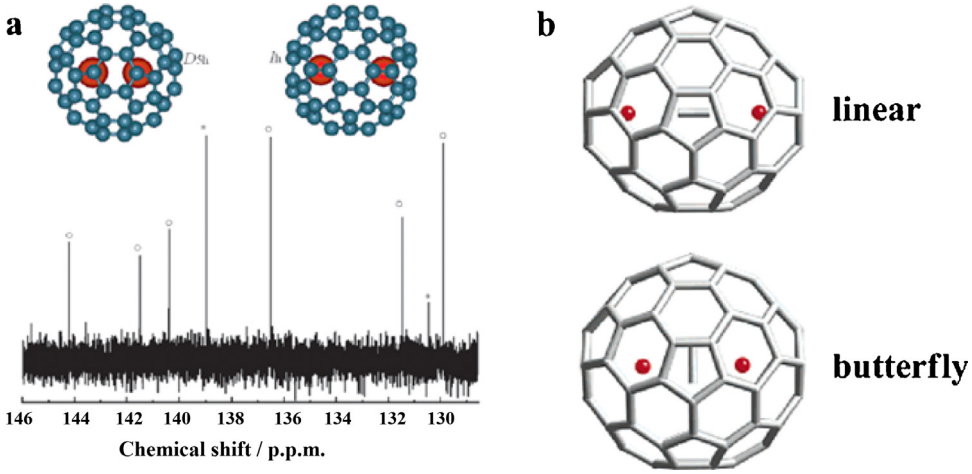

Fig. 5. (a) ^{13}C NMR spectrum and structures of two $Ti_2@C_{80}$ isomers. (b) DFT-optimized geometries of $Ti_2C_2@D_{3h}$(24109)-C_{78}. Reprinted with permission from Ref. [67]. Copyright 2001 American Chemical Society (a). Adapted with permission from Ref. [22]. Copyright 2005 American Chemical Society (b).

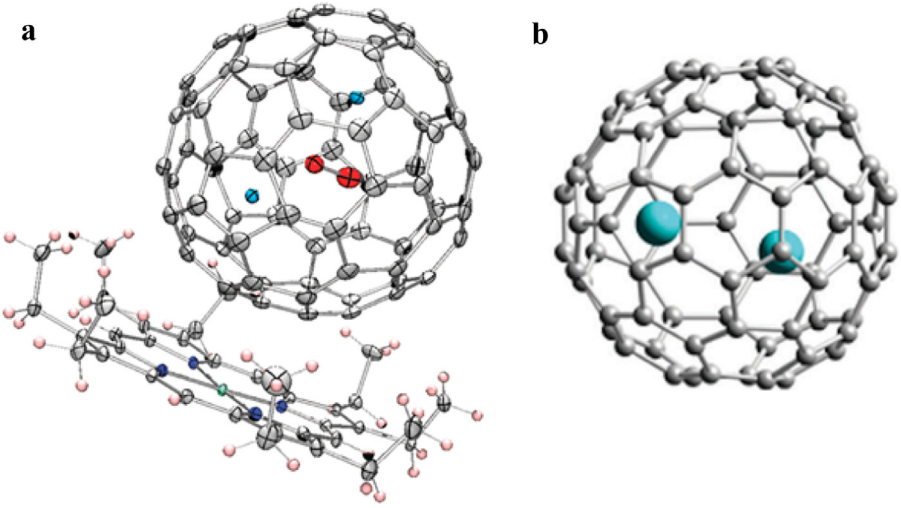

Fig. 6. (a) $Sc_2C_2@C_{2v}(31922)$-C_{80}·Co(OEP)·2$CHCl_3$. (b) optimized structure of $Sc_2@C_{3v}(39717)$-C_{82}.
Reprinted with permission from Ref. [55]. Copyright 2012 American Chemical Society (a). Reproduced from Ref. [78] with permission of The Royal Society of Chemistry (b).

microscopy (HRTEM) clearly visualized two configurations for the inner Ti_2C_2 cluster, indicating the coexistence of linear and butterfly shapes. The good agreement between the measured ultraviolet photoelectron spectra (UPS) and the simulated density of state (DOS) based on the $D_{3h}(24109)$-C_{78} cage also supported the above isomer assignments [74].

In addition to Ti, recent DFT computations suggested that two heavier Group IV elements, Zr and Hf [75], may form similar carbide clusterfullerenes, $Zr_2C_2@D_{3h}$-C_{78} and $Hf_2C_2@D_{3h}$-C_{78} [25].

2.5. $Sc_2@C_{82}$ vs. $Sc_2C_2@C_{80}$

Similar to the case of Sc_2C_{80}, the coexistence of MCCFs and di-EMFs was also disclosed for Sc_2C_{82} and Gd_2C_{94}.

Along with Sc_2C_{86}, Sc_2C_{82} was first synthesized, isolated and spectroscopically characterized by Shinohara's group, and two distinct isomers (I, II) were identified [46,47,76]. A $Sc_2@C_{82}$ model with the two Sc atoms along the C_2 axis of a $C_2(39712)$-C_{82} cage was initially assumed for Sc_2C_{82} (I) in their computational study [47]. Recently, Sc_2C_{82} (I) was conclusively reassigned as $Sc_2C_2@C_{2v}(31922)$-C_{80} by Akasaka and coworkers' ^{13}C NMR spectroscopy and X-ray crystallographic study (Fig. 6a) [26,55,77]. They further characterized Sc_2C_{82} (II) as a classical $Sc_2@C_{3v}(39717)$-C_{82}, which, as the authors underscored, is the first ascertained scandium dimetallofullerene (Fig. 6b) [78]. The $Sc_2C_{82}^+$ ion presented two distinct peaks in the early ion mobility measurement, implying that two cages of different sizes coexisted [66].

For Gd_2C_{94}, two distinct isomers were successfully isolated [44]. Isomer I was revealed by an X-ray crystallography study as a $Gd_2C_2@D_3(126408)$-C_{92} (Fig. 7), whereas isomer II was proposed to be a conventional $Gd_2@C_2(153480)$-C_{94} which is lower in energy according to the DFT calculations [44].

2.6. $Sc_3@C_{82}$ vs. $Sc_3C_2@C_{80}$

The first synthesis and isolation of Sc_3C_{82} was independently reported by two groups through arc discharge of Sc-impregnated graphite rods in 1992 [76,79]. They both suggested a $Sc_3@C_{82}$ structure with an equivalent Sc trimer [80] confined in a C_{82} cage. Afterwards, numerous studies were conducted by adopting this simple model, including ESR/EPR [81–88], electrochemical measurement [89,90], synchrotron X-ray diffraction [91], and theoretical calculations [92,93]. Fig. 8a depicts the schematic representation with a triangular Sc_3 (Sc–Sc distance: 2.3 Å) encased in a $C_{3v}(39716)$-C_{82} from the MEM/Rietveld analysis [91] (though it may not be the lowest-energy isomer of $Sc_3@C_{82}$ [93]). Because Sc_3C_{82} is a paramagnetic radical in the neutral state, Akasaka and coworkers measured the ^{13}C NMR spectrum of the $(Sc_3C_{82})^-$ anion in acetone-d_6/CS_2 solution. Instead of having 16 lines as expected for a C_{3v}–C_{82} cage, the ^{13}C NMR spectrum showed only two peaks [27], which were similar to that of $Sc_3N@I_h(31924)$-C_{80}, indicating that Sc_3C_{82} has the same parent I_h-C_{80} cage [11]. The single crystal X-ray analysis of the adamantylidene carbene (Ad) adduct of Sc_3C_{82} unambiguously verified that it is an I_h-C_{80} cage enclosing a Sc_3C_2 unit (Fig. 8b). In Shinohara et al.'s early ion mobility measurement, only one peak with a shorter drift time was observed for the $Sc_3C_{82}^+$ ion, which was the first clue of its smaller cage compared to C_{82} [66]. $Sc_3C_2@C_{80}$ has an open-shell radical nature. DFT calculations revealed that Sc_3C_2 transfers almost six electrons to the C_{80} and achieves a closed-shell structure on the cage [27], obeying the stable closed-shell electronic configuration rule (CSECR) [94,95]. Its electronic configuration can be described as $(Sc^{3+})_3(C_2)^{3-}@C_{80}^{6-}$ [96]. More detailed synchrotron X-ray analysis confirmed the $Sc_3C_2@C_{80}$ structure [28], although the same method previously suggested it as $Sc_3@C_{82}$, most likely due to an

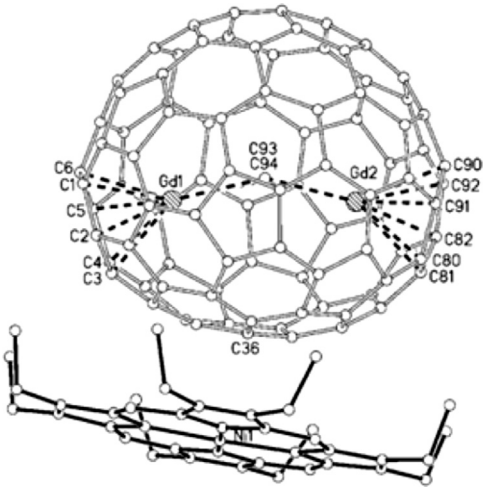

Fig. 7. $Gd_2C_2@D_3(126408)$-C_{92}·Ni(OEP).
Reprinted with permission from Ref. [44]. Copyright 2008 American Chemical Society.

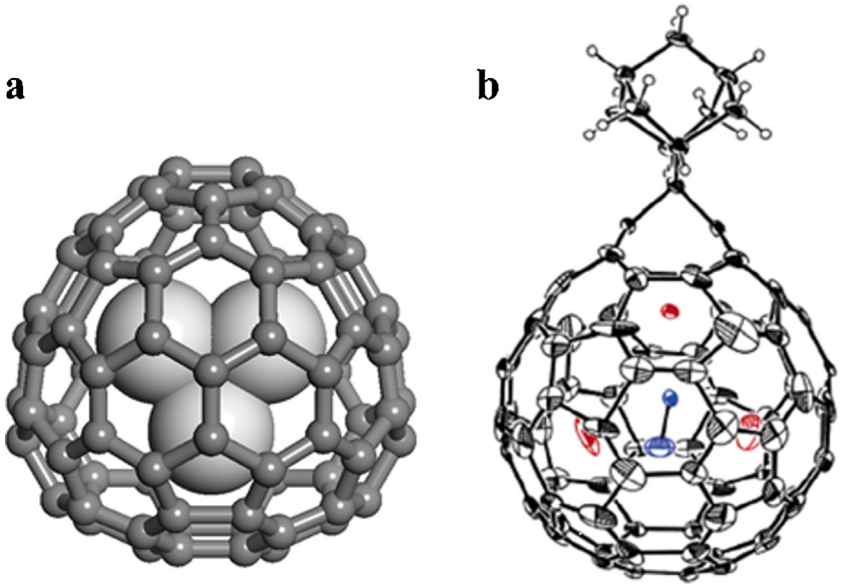

Fig. 8. (a) A schematic representation of the structure model of $Sc_3@C_{82}$ determined by Rietveld analysis from Ref. [91]. (b) ORTEP drawing of the X-ray single-crystal structures of $Sc_3C_2@C_{80}$(Ad).
Reprinted with permission from Ref. [27]. Copyright 2005 American Chemical Society.

incorrect structural model and low resolution [91]. Similar to a low-energy isomer in previous DFT results [96], the MEM/Rietveld analysis showed that the Sc_3C_2 cluster resides on the cyclacene-like belt of the C_{80} cage (Sc-Sc distance: 3.61 Å) with a C_2 unit at the cage center. Its endohedral carbide structure was further supported by observing that there was no cross-peak between the C_2 chemical shift and the two lines from the I_h-C_{80} cage in a recent 2D INADEQUATE (incredible natural abundance double quantum transfer experiment) NMR spectrum of ^{13}C-enriched $[Sc_3C_2@I_h\text{-}C_{80}]^-$ [50].

Although "$Sc_3@C_{82}$" has been convincingly proven to be an MCCF $Sc_3C_2@C_{80}$, attempts to trap three metals in the cage without any exotic mediator were pursued. The recent study combining both DFT calculations and mass spectroscopy suggested an $Y_3@I_h$-C_{80} structure for the Y_3C_{80} composition produced by the reactive atmosphere method [97]. Xu et al. synthesized and isolated a $Sm_3@I_h$-C_{80} molecule, which was subsequently characterized as the first tri-EMF molecule by XRD [98]. The DFT calculations revealed that both $Y_3@I_h$-C_{80} and $Sm_3@I_h$-C_{80} possess a non-nuclear attractor (or pseudoatom) at the cage center, which bonds to and helps stabilize the surrounding metals. This raises the question of which class do the previously reported Er_3C_{74} [99], Tb_3C_{80} [100], and Dy_3C_{98} [101] belong to: MCCFs or tri-EMFs? This question has not yet been answered.

After $Sc_3C_2@C_{80}$, the second tri-metal MCCF $Lu_3C_2@D_2(81738)$-C_{88} was prepared, isolated and spectroscopically characterized by Xu et al. in 2011 [41]. It was relatively stable as the HPLC retention time and UV-vis spectrum remained unchanged after three months. The low energy Raman spectrum exactly matches $Lu_3N@C_{88}$, $Y_3N@D_2$-C_{88}, and $Gd_3N@D_2$-C_{88} [102], suggesting that it bears the same D_2-C_{88} framework. According to DFT computations [41,103], the Lu_3C_2 cluster adopts an almost planar geometry inside the $D_2(81738)$-C_{88} cage (Fig. 9). An unpaired electron remained on the inner cluster after transferring 6 *e* to the C_{88} cage, resulting in an open-shell $(Lu^{3+})_3C_2^{3-}@C_{88}^{6-}$ electronic configuration.

2.7. $Sc_4@C_{82}$ vs. $Sc_4C_2@C_{80}$

As a byproduct in the synthesis of Sc_2C_{82} and Sc_2C_{86}, Sc_4C_{82} was first reported by Shinohara's group in 1999 [47]. Its candidate formula of a metal carbide endofullerene, $Sc_4C_2@C_{80}$, was predicted by DFT computations in 2006 [96,104]. According to the theoretical results, a C_2 moiety preferentially resides at the center of the Sc_4 tetrahedron in a μ_4 coordinated manner within the I_h-C_{80} cage. Thus, the whole molecule resembles an angstrom-scale Russian doll: $C_2@Sc_4@I_h$-C_{80}. $Sc_4C_2@C_{80}$ features a closed-shell electronic configuration and is energetically more favorable than the possible $Sc_4@C_{3v}$-C_{82} isomers by >45 kcal/mol. Shortly after the theoretical conjecture, this novel MCCF was successfully synthesized, isolated, and characterized by Wang et al. by means of mass spectrometry, UV–vis, FTIR, and ^{13}C NMR measurements, as well as DFT calculations [29]. The two lines observed at 137.8 and 144.7 ppm (1:3 intensity ratio) in the ^{13}C NMR measurement undoubtedly demonstrated the carbon framework as I_h-C_{80}, not a C_{82} isomer (Fig. 10). This structure assignment was consistent with Krokos's further experimental elucidation [63]. Although it is the largest encased cluster for EMFs reported thus far, the inner Sc_4C_2 unit may still freely rotate within the cage due to the large interior cavity and smooth potential surface (barrier: 2.8 kcal/mol); thus, it will not disturb the symmetry of the parent C_{80} cage [104]. Nevertheless, a more recent DFT study on this molecule argued that the Sc_4C_2 rotation at room temperature could be hindered by a relatively large energy barrier (ca. 13.1 kcal/mol) [105,106].

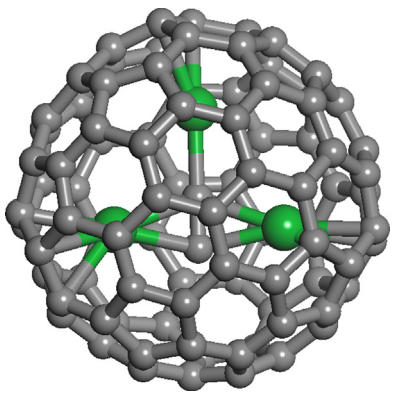

Fig. 9. Optimized $Lu_3C_2@D_2(81738)$-C_{88} structure from Ref. [103].

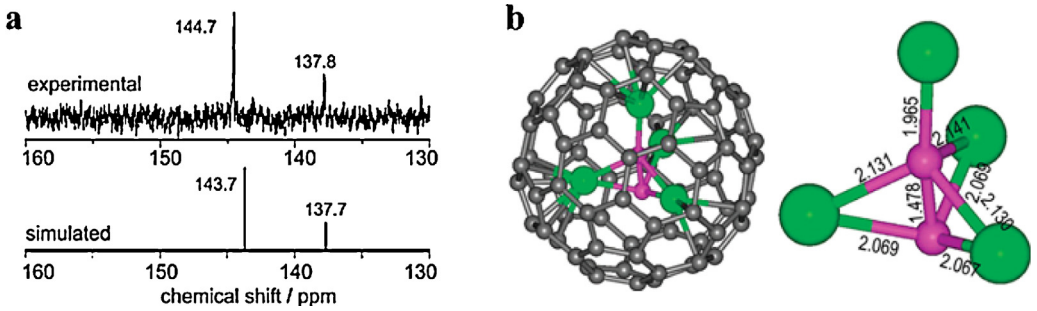

Fig. 10. (a) (top) Experimental (CS_2, 150 MHz, 293 K) and (bottom) simulated ^{13}C NMR spectra of the I_h-C_{80} cage in Sc4C2@Ih-C80. (b) (left) DFT-optimized structure of $Sc_4C_2@I_h$-C_{80} and (right) calculated Sc–C and C–C bond lengths (Å) in the encaged Sc_4C_2 moiety.
Adapted with permission from Ref. [29]. Copyright 2009 American Chemical Society.

Recent DFT computations suggested that it is feasible to obtain a non-transition metal carbide $C@Al_4@I_h$-C_{80} nesting structure (Fig. 11) [107]. The structure is expected to exhibit novel properties that are different from transition metal clusterfullerenes.

2.8. $Sc_2@C_{84}$ vs. $Sc_2C_2@C_{82}$

Three Sc_2C_{84} isomers (I, II, III) have been isolated, and the third is the most abundant [76,108]. The ^{13}C NMR studies observed 46, 24, and 11 lines for Sc_2C_{84}(I), Sc_2C_{84}(II) and Sc_2C_{84}(III), respectively. Correspondingly, $Sc_2@C_s$(51578)-C_{84}, $Sc_2@C_{2v}$(51585)-C_{84} and $Sc_2@D_{2d}$(51591)-C_{84} structures were proposed (Fig. 12a) [108,109]. Numerous early studies including STM [110,111], TEM [112], ^{13}C NMR [108], X-ray photoelectron spectroscopy [113], ^{45}Sc NMR [114], IR [115], Raman [116–118], and theoretical calculations [59,119,120] took the assumed $Sc_2@C_{84}$ for granted. The intramolecular structures were demonstrated by both MEM/Rietveld analysis [121] and HRTEM study [122].

In sharp contrast, an improved ^{13}C NMR measurement conducted by Akasaka and coworkers in 2006 showed 17 lines, including 11 full-intensity, 5 half-intensity and one 1/6 intensity, but not the signal for the carbide C_2 unit [50] for Sc_2C_{84}(III) [30]. This ^{13}C NMR spectrum precluded any of the 24 IPR C_{84} cages. The close similarity between the visible-NIR and ^{13}C NMR spectra and the previously reported $Y_2C_2@C_{3v}$(39717)-C_{82} (vide infra) led to the conclusion that the Sc_2C_{84}(III) was not $Sc_2@C_{84}$ but $Sc_2C_2@C_{3v}$(39717)-C_{82}. The 2D INADEQUATE NMR spectra revealed the absence of a cross-peak between the ^{13}C chemical shifts of the C_2 unit and those of the cage carbons, suggesting its isolation from the carbon framework [50]. The refined MEM/Rietveld analysis supported this metal carbide structure [123]. The recent X-ray single-crystal analysis on its carbene derivative and cocrystals with metal porphyrin, as well as DFT calculations, conclusively demonstrated its endohedral carbide nature, and its electronic configuration is described as $(Sc_2C_2)^{4+}@{C_{82}}^{4-}$ (Fig. 12b) [55,124,125]. Two minor isomers, Sc_2C_{84}(I) and Sc_2C_{84}(II), were assigned as $Sc_2C_2@C_s$(39715)-C_{82} and $Sc_2C_2@C_{2v}$(39718)-C_{82}, respectively, by means of both NMR spectroscopy and X-ray crystallography (Fig. 12b) [31,32], and not the previously assumed $Sc_2@C_s$(51578)-C_{84} and $Sc_2@C_{2v}$(51585)-C_{84} [109]. Therefore, all three isolated Sc_2C_{84} isomers have been classified into the MCCF family.

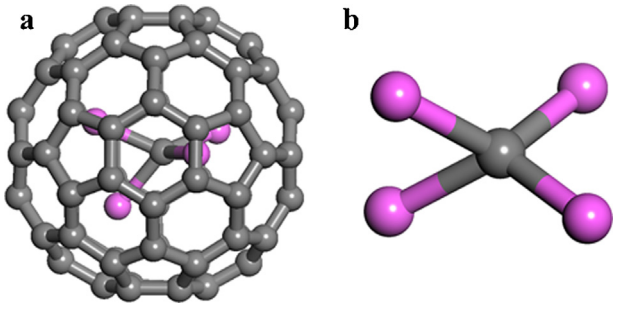

Fig. 11. Optimized structures of $Al_4C@I_h$(31924)-C_{80} and the trapped Al_4C cluster from Ref. [107].

2.9. $Y_2@C_{84}$ vs. $Y_2C_2@C_{82}$

As the second MCCF and the first diyttrium MCCF, one Y_2C_{84} isomer (III), $Y_2C_2@C_{82}$ was produced and characterized by Shinohara's group in 2003 [33]. The ^{13}C NMR measurement showed 17 distinct lines (11 full, 5 half, and 1 1/6 intensity), thus precluding any possibility of an IPR C_{84} cage. The C_{3v}(39717)-C_{82} isomer was chosen as the candidate to satisfy the NMR observation, and an endohedral Y_2C_2 was proposed, for which no ^{13}C NMR signals are available in this first report. Holding a similar spherical structure as I_h-C_{80}, this cage may endow the Y_2C_2 moiety to freely rotate inside the cage due to the flat electrostatic potential [93]. Thus, the C_{3v} symmetry of the whole system does not decrease. Similarly, two other isomers, $Y_2C_2@C_{82}$ (I, II), were characterized by means of ^{13}C NMR measurements, and their cages were assigned as C_s(39715)-C_{82} and C_{2v}(39718)-C_{82}, respectively [34]. In total, 4 *e* charge may transfer from the Y_2C_2 cluster to the C_{82} cage [37]. Thus, as Sc_2C_{84}, all the Y_2C_{84} (I, II, III) isomers reported so far are MCCFs (Fig. 13).

The cage structure of $Y_2C_2@C_{82}$(III) was further verified by the good agreement between experimentally measured and theoretically simulated UPS based on the $Y_2C_2@C_{3v}$(39717)-C_{82} model [126]. The MEM charge density confirmed its carbide endofullerene structure but suggested a different formal electronic structure of $(Y_2C_2)^{+5.6}@{C_{82}}^{-5.6}$ [123,127]. With the C_2 inside, the hopping of Y_2 exhibits a pentagonal-dodecahedral charge density. Theoretical computations showed that $Y_2C_2@C_{3v}$-C_{82} is lower in energy than $Y_2@D_{3d}$-C_{84} and supported the ionic nature for the interaction between Y_2C_2 and the cage [128].

2.10. Other clusterfullerenes containing two entrapped carbons

The discoveries of MCCFs are not limited to the above cases. One intriguing case is $Y_2C_2@C_{84}$, which was recently synthesized and isolated by Dorn and coworkers [37]. Although the poor signal-to-noise ratio of the measured ^{13}C NMR spectrum hindered the cage symmetry assignment, a plausible low-symmetric non-IPR cage was suggested following the ^{13}C NMR observation of at least 70 lines (84 peaks of nearly equal intensity in the latest report [39]) in the aromatic region and two highly deshielded peaks (161.7 and 160.6 ppm), which are typical for fused pentalene carbons. After an exhaustive cage isomer search, Yang et al. theoretically assigned an IPR-violating C_1(51383)-C_{84} (Fig. 14a) as the observed cage, mainly based on its overwhelming thermodynamic stability within the temperature region for EMFs formation (500–3000 K) [38]. In sharp contrast to the D_{2d}(51591) cage of

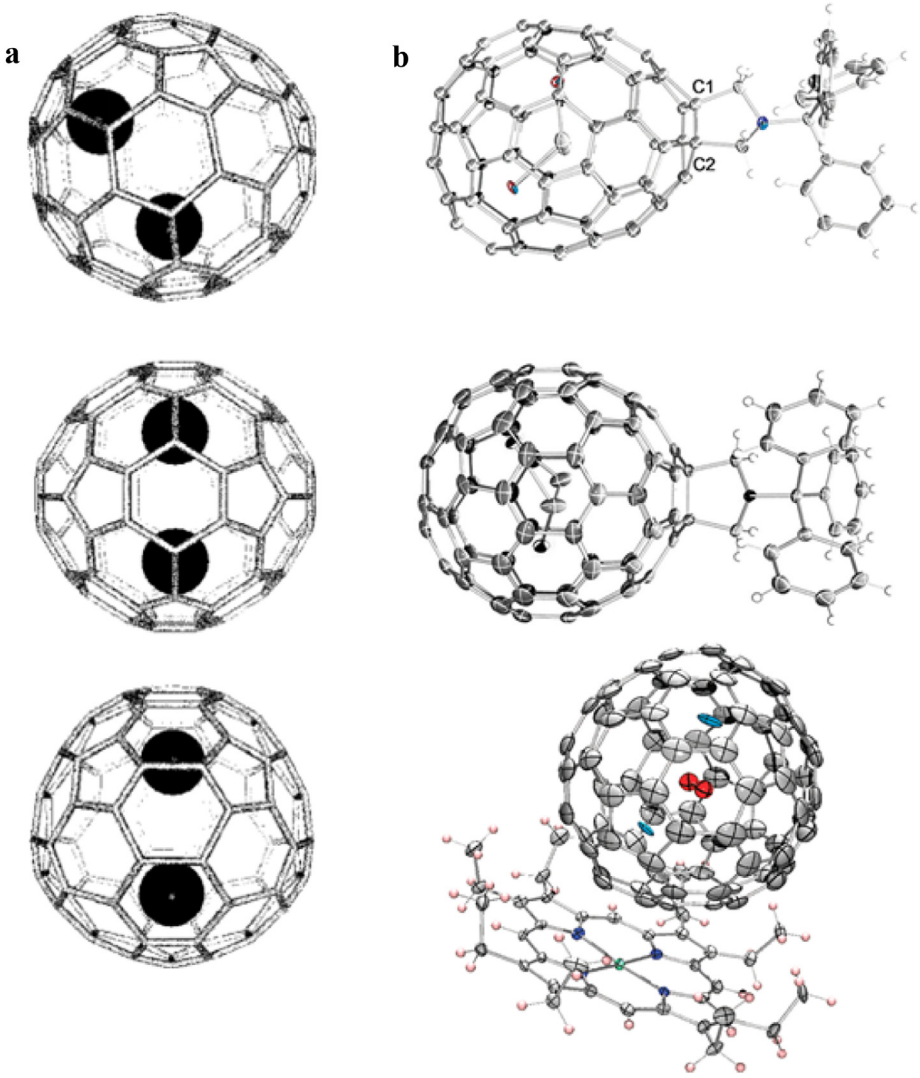

Fig. 12. (a) Molecular structures of $Sc_2@C_{84}$ (I, II, III). (b) pyrrolidino derivatives of (top) $Sc_2C_2@C_s(39715)$-C_{82} and (middle) $Sc_2C_2@C_{2v}(39718)$-C_{82} as well as (bottom) $Sc_2C_2@C_{3v}(39717)$-C_{82}·Co(OEP)·$2CHCl_3$.

Reprinted with permission from Ref. [109]. Copyright 2000 American Chemical Society (a). Reprinted with permission from Ref. [31]. Copyright 2011 American Chemical Society (b top). Reprinted with permission from Ref. [32]. Copyright Wiley-VCH 2012 (b middle). Reprinted with permission from Ref. [55]. Copyright 2012 American Chemical Society (b bottom).

$Sc_2C_2@C_{84}$, $Y_2C_2@C_1(51383)$-C_{84} features one pair of fused pentagons: one yttrium ion is located close to the pentagon fusion, whereas the other resides on a hexagonal ring, violating the IPR rule. Though a possible $Y_2C_2@D_{2d}(51591)$-C_{84} structure (Fig. 14b) is the lowest-energy isomer at low temperature (4.9 kcal/mol lower than $Y_2C_2@C_1(51383)$-C_{84}), its concentration decreases dramatically at high temperatures. The carbide structure of $Y_2C_2@C_1(51383)$-C_{84} was strongly supported by its similarity to the XRD-characterized $Gd_2C_2@C_1(51383)$-C_{84} (Fig. 14c) in both retention time and UV-vis spectra. Thus, in addition to the confirmed $Sc_2C_2@C_s(10528)$-C_{72}, $Gd_2C_2@C_1(51383)$-C_{84}, and the plausible $Sc_2C_2@C_{2v}(6073)$-C_{68}, $Y_2C_2@C_1(51383)$-C_{84} is a another promising new non-IPR MCCF.

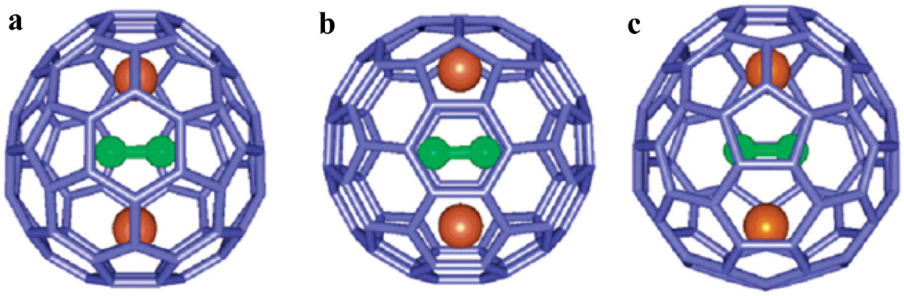

Fig. 13. Molecular structures of $Y_2C_2@C_{82}$ (I, II, III).

Adapted with permission from Ref. [34]. Copyright 2004 American Chemical Society.

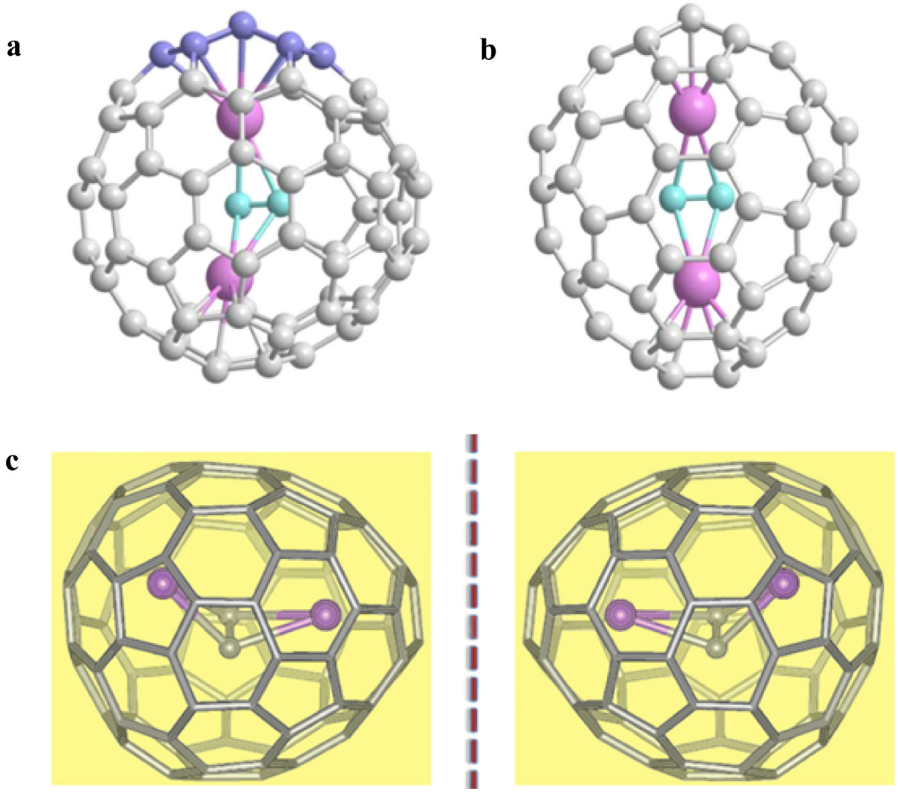

Fig. 14. Optimized structures of (a) $Y_2C_2@C_1(51383)$-C_{84} and (b) $Y_2C_2@D_{2d}(51591)$-C_{84}. (c) X-ray single-crystal results for $Gd_2C_2@C_1(51383)$-C_{84} enantiomers. Reprinted with permission from Ref. [38]. Copyright 2012 American Chemical Society (a and b). Reprinted by permission from Macmillan Publishers Ltd: [Nature Chemistry] (Ref. [39]). Copyright 2013 (c).

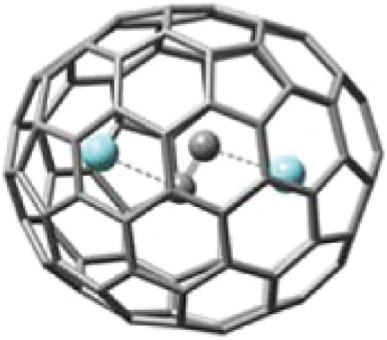

Fig. 15. Optimized structure of $Y_2C_2@D_3(126408)$-C_{92}. Reprinted with permission from Ref. [37]. Copyright 2012 American Chemical Society.

$Y_2C_2@C_{92}$ was first prepared in Dorn's group [129]. The Raman spectrum of $Y_2C_2@C_{92}$ is analogous to that of $Gd_2C_2@D_3(126408)$-C_{92} for the cage modes above 300 cm^{-1}, suggesting their similar carbon skeletons [43]. The cage symmetry was confirmed by 200 MHz ^{13}C NMR measurements [37]. Fig. 15 depicts the DFT optimized $Y_2C_2@D_3(126408)$-C_{92}, in which two Y ions slightly deviate from the C_3 axis of the cage.

Aside from the sensitive ^{13}C NMR and powerful XRD, UV–vis–NIR absorption spectra often play an important role in identifying different isomers of MCCFs. The electronic spectra of EMFs mostly depend on the cage geometry and charge state, irrespective of the internal species [3]. One successful case is the structural characterization of the only di-erbium MCCF, $Er_2C_2@C_{82}$, of which three isomers (I, II, III) were isolated in Shinohara's group, the third isomer being the most abundant [36,130]. Their cage symmetries were identified as C_s(39715), C_{2v}(39718), and C_{3v}(39717), respectively, due to the close resemblance of their absorption

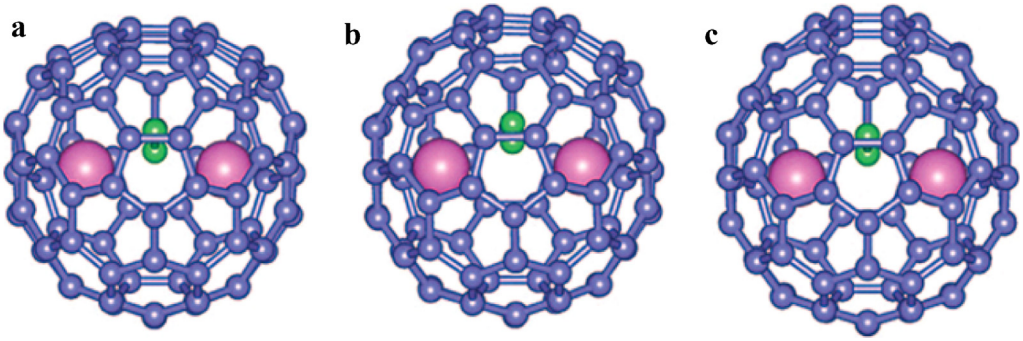

Fig. 16. Schematic molecular structures of $Er_2C_2@C_{82}$(I, II, III). Adapted with permission from Ref. [36]. Copyright 2007 American Chemical Society.

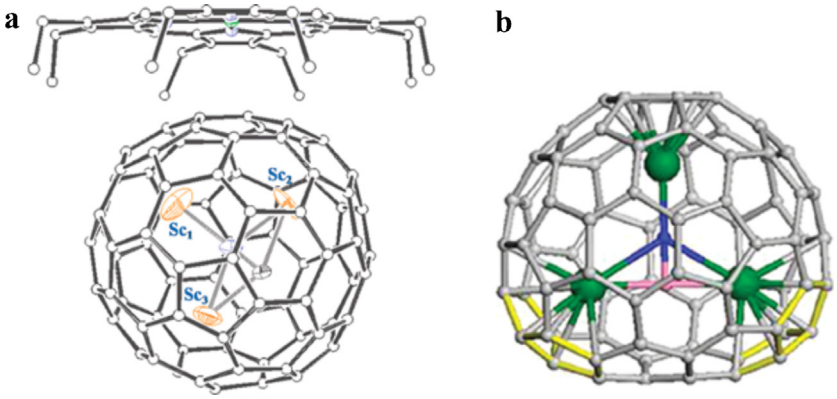

Fig. 17. (a) Structure of $Sc_3NC@I_h(31924)$-C_{80}·Ni^{II}(OEP)·1.5C_6H_6. (b) Optimized structure of $Sc_3NC@C_2(22010)$-C_{78} (The carbon atoms in two pairs of adjacent pentagons are denoted by the yellow color).

Reprinted with permission from Ref. [15]. Copyright 2010 American Chemical Society (a). Reprinted with permission from Ref. [135]. Copyright 2011 American Chemical Society (b).

spectra to $Sc_2C_2@C_{82}$(I, II, III) and $(Y_2C_2)@C_{82}$(I, II, III) [34,36,109] (Fig. 16). A mixed metal carbide $ErYC_2@C_{82}$ was also prepared and isolated [35]. By means of UV spectroscopic comparison, $ErYC_2@C_{82}$ was suggested to bear the same C_s(39715) cage as $Er_2C_2@C_{82}$(I). The same spectral features suggested the three isomers (I, II, III) of Dy_2C_{84} [131] were $Dy_2C_2@C_s$(39715)-C_{82}, $Dy_2C_2@C_{2v}$(39718)-C_{82}, and $Dy_2C_2@C_{3v}$(39717)-C_{82}, respectively [33,34]. On the other hand, Er_2C_{94}(I) [99] and Dy_2C_{94}(I) [101] were identified as $Er_2C_2@D_3$(126408)-C_{92} and $Dy_2C_2@D_3$(126408)-C_{92}, respectively, due to the similarity to the well-defined $Gd_2C_2@D_3$(126408)-C_{92} of the adsorption spectra [44]. Moreover, Gd_2C_{90} and Gd_2C_{92} were suggested to be $Gd_2C_2@D_2$(81738)-C_{88} and $Gd_2C_2@C_1$(99893)-C_{90}, respectively, because their UV–vis–NIR spectra are almost identical to $Sm_2@D_2$(81738)-C_{88} and $Sm_2@C_1$(99893)-C_{90} [132].

2.11. Other clusterfullerenes containing one entrapped carbon

In addition to the typical MCCFs discussed above, metal nitrogen carbide (or metal cyanide) EMFs, such as $Sc_3NC@C_{80}$, were also achieved in recent years [15]. In 2010, according to the signal of m/z = 1121 observed by Dorn and coworkers in their mass spectrum, Jin et al. first theoretically characterized a novel EMF with an I_h-C_{80} cage encapsulating an unusual quinary Sc_3NC unit using systematic DFT calculations [133]. In contrast to conventional TNT EMFs, this molecule energetically favored the carbon in the cage center rather than the normal N atom. To explore the cage size limit to accommodate this metal cyanide cluster, the authors continued their exploration by decreasing to C_{78} and even the "tiny" C_{68} and suggested great possibilities for realizing $Sc_3NC@C_{78}$ and $Sc_3NC@C_{68}$.

Shortly after the theoretical report, Wang et al. successfully synthesized and unambiguously characterized the structure of $Sc_3NC@C_{80}$ by XRD (Fig. 17a) [15]. In contrast to the DFT results regarding the center atom type, however, X-ray diffraction data showed an N instead of C core for the planar Sc_3NC cluster. Recent ESR simulations of the $Sc_3NC@C_{80}$ anion based on the C-centered model led to hyperfine coupling constants (hfcc) closer to the observation than the N-centered model, and thus supported the theoretical predictions of the early DFT calculations [134].

$Sc_3NC@C_{78}$ was synthesized and characterized as holding a non-IPR C_2(22010)-C_{78}, in which two Sc ions are situated near two adjacent pentagon pairs (Fig. 17b) [135].

Although the experimentally realized M_3NC-template clusterfullerenes are still limited to $Sc_3NC@C_{78}$ and $Sc_3NC@C_{80}$, new members, especially some bearing larger cages, are anticipated. Sc_3NC was recently suggested stable in D_{5h}(31923)-C_{80} [136], D_{2d}(51591)-C_{84} and even non-IPR C_s(51365)-C_{84} cages by DFT calculations [137].

Using the arc burning method in a reactive CH_4 atmosphere, Dunsch's team synthesized and characterized the first

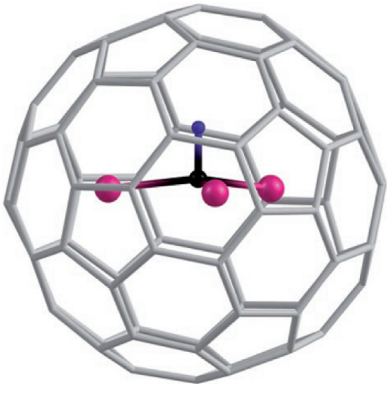

Fig. 18. Optimized structure of $Sc_3CH@C_{80}$ (Gray: C_{80} cage atoms; black: carbon atom of the Sc_3CH cluster; pink: scandium atoms; blue: hydrogen atom).

Reprinted with permission from Ref. [14]. Copyright Wiley-VCH 2007.

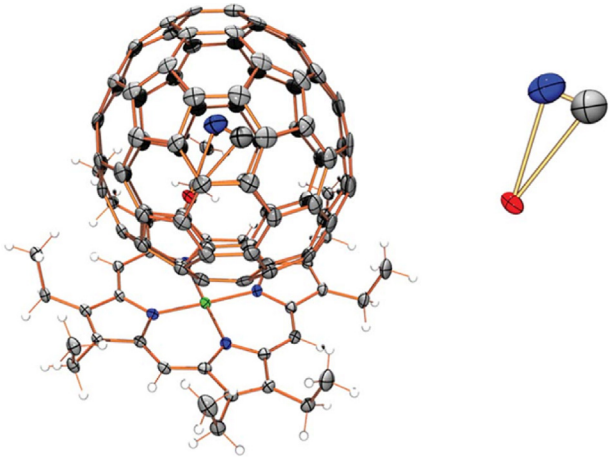

Fig. 19. Drawing of the crystallographically determined structure of $YCN@C_s$(39715)-C_{82} with the major C_{82} cage (0.55 occupancy) and the most abundant yttrium location (0.50 occupancy), and its relation to the Ni^{II}(OEP) molecule (inset shows the triangular configuration of the internal YCN cluster. Red: Y; Blue: N; Gray: C).

Reprinted by permission from Macmillan Publishers Ltd: [Scientific Reports] (Ref. [139]). Copyright 2013.

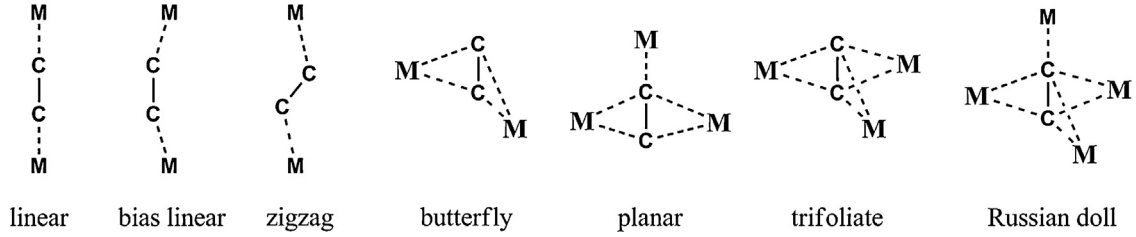

Scheme 1. Reported geometries for the metal carbide moiety in MCCFs.

hydrogenated metal carbide $Sc_3CH@I_h$-C_{80} [14]. DFT calculations suggested an isomer with a slightly pyramidal Sc_3CH cluster in the C_{80} cage as the lowest-energy structure (Fig. 18) among different candidates. The structure of $Sc_3CH@C_{80}$ resembles $Sc_3N@C_{80}$ and exhibits a closed-shell electronic configuration with a large HOMO (highest occupied molecular orbital)–LUMO (lowest unoccupied molecular orbital) energy gap (1.7 eV). In contrast to previous homonuclear molecular hydrogen in C_{60} [138], the hydrogen atom in the Sc_3CH cluster is stabilized due to its chemical bonding with the Sc_3C moiety. Featuring a carbon core at the cage center surrounded by metals, $Sc_3CH@I_h$-C_{80} represents a brand-new type of carbide clusterfullerene.

All the clusterfullerenes reported so far need at least two metal atoms to stabilize the otherwise labile clusters. It has long been believed that mono-EMFs only exist as $M@C_{2n}$. This belief was overthrown by Yang et al.'s synthesis and structural characterization of the monometallic clusterfullerene, $YCN@C_s(39715)$-C_{82} [139]. Single crystal XRD data revealed an unusual triangular YCN cluster, though the $C_s(39715)$-C_{82} cage is spacious enough to accommodate a more relaxed linear configuration (Fig. 19). This indicates strong coordination interactions between yttrium and the CN moiety inside the confined cavity. Its remarkable stability might be ascribed to a closed-shell electronic configuration $[Y^{3+}(CN)^-]^{2+}C_{82}{}^{2-}$, as suggested by XPS, ESR and cyclic voltammetric studies. The discovery of $YCN@C_s(39715)$-C_{82} has opened a brand-new era for clusterfullerene research. After Yang et al.'s pioneering study, more new monometallic clusterfullerenes will likely be realized and will enrich the mono-EMFs family in the near future.

3. Novel structures and cluster–cage interplay

MCCFs with various cages ranging from C_{68} to C_{92} and even C_{100} have been experimentally demonstrated or theoretically suggested. Both IPR-satisfying and IPR-violating carbon frameworks are involved. Compared with the diversity of conventional EMFs, however, the metals in MCCFs are still limited to Sc, Ti, Y, Gd, Dy, Er, and Lu. Among them, Sc is especially favorable to the formation of clusterfullerene, mainly due to its small ionic radius and strong coordination ability. Combining the inner C_2 unit with two, three or four metal ions, the largest cluster size trapped in MCCFs has currently reached six in $Sc_4C_2@C_{80}$ [29].

3.1. Compressed metal carbide clusters

Metal carbide clusters can exhibit diverse shapes in the fullerene hollows. Scheme 1 summarizes all possible structures for the clusters reported thus far.

For di-MCCFs, we assume that the M_2C_2 unit is of a linear or a butterfly shape. A perfect linear shape is scarce, only $Ti_2C_2@C_{80}$ was theoretically suggested to adopt this configuration [22,25]. In comparison, the butterfly shape, which features a C_2 motif perpendicular to the line of two metal atoms, is very common in the congested interior (Table 2). A bias linear ($Sc_2C_2@C_{90}$ [40] and $Y_2C_2@C_{100}$ [37]) or a zigzag shape ($Hf_2C_2@C_{78}$ [25], $Sc_2C_2@C_{86}$ [40], and $Y_2C_2@C_{92}$ [37]) is often favored when the cage size is sufficiently spacious to accommodate the M_2C_2 unit. The zigzag configuration may serve as the transition state connecting the linear and butterfly modes [22].

For tri-MCCFs, the M_3C_2 cluster can assume a planar or trifoliate shape (Scheme 1). The trifoliate configuration, in which the C_2 axis at the center is perpendicular to the M_3 plane, is only found in $Sc_3C_2@C_{80}$ [25,26,82], whereas the more relaxed planar shape is always preferred within a larger cage, such as $Lu_3C_2@C_{88}$ [41]. The nesting peculiarity of the Russian doll shape requests a minimum M_4 subshell surrounding the C_2 core; thus, it is only applicable for $Sc_4C_2@C_{80}$ [29] and a plausible $Al_4C@C_{80}$ [107].

The cage size dictates the shape of a metal carbide cluster. Consistent with our intuition, small carbon cages induce more compression, and thus a more bent cluster structure inside the cage. For example, freestanding Y_2C_2 favors the linear ground state for both neutral and tetracation. When encapsulated into cages as large as C_{100}, Y_2C_2 adopts a bias linear structure, whereas upon encapsulation into C_{82}, C_{84}, and C_{92}, Y_2C_2 has a butterfly shape [37,128,140]. Both the Y–C and Y–Y distances of the $(Y_2C_2)^{4+}$ cluster are shortened as the cage size decreases [37]. Likewise, the butterfly structure of the Sc_2C_2 cluster preferentially becomes more bent as the cage changes from D_{2d}-C_{84} to C_{3v}-C_{82} and C_{2v}-C_{80}, as indicated by the decreased Sc–Sc distances and the Sc–C_2–Sc dihedral angles [55]. In other words, the metal carbide cluster always tends to pursue a more stretched geometry as long as the inner space is large enough.

On the other hand, the size of the endohedral metal ion affects the cluster structure. For the Group IV elements, the ionic radius is ordered as $Ti^{4+} < Hf^{4+} < Zr^{4+}$ [141]. DFT calculations elucidated that the M_2C_2 cluster in $M_2C_2@C_{78}$ preferentially adopts a linear geometry for M = Ti, a zigzag geometry for M = Hf, and a butterfly geometry for M = Zr [25].

3.2. Expanded and distorted cages

The interior spaces of fullerenes exert considerable influences on the geometries of the encapsulated species and vice versa. For example, the C_{78} cage in $Sc_2C_2@C_{78}$ increases from 7.51 Å for $C_{78}{}^{4-}$ to 7.90 Å upon Sc_2C_2 cluster encapsulation [21]. The linear TiC-CTi cluster on the C_3 axis of D_{3h}-C_{78} induces substantial strain on the cage, which expands along the axis (8.236 Å) in reference to pristine C_{78} (8.051 Å) [22], and the DFT computed deformation energy for the fullerene cage is 39.6 kcal/mol [143]. C_{84} slightly expands upon Sc_2C_2 cluster insertion, with the polar carbon atoms at hexagon fusions close to the Sc atoms punched out [54]. To enhance the metal–cage interactions, the Sc–Sc and C–C distances of the butterfly-like Sc_2C_2 moiety become longer and shorter, respectively. The strain due to the cluster encapsulation may be partially reflected by Raman spectroscopy. For example, Wang et al. observed cage mode splittings in the low-energy Raman spectrum of $Sc_4C_2@I_h$-C_{80}, which imply substantial distortion of the C_{80} cage due to Sc_4C_2 insertion [29].

Table 2
Summary of reported geometries, electronic configurations, and motions of carbide clusters in MCCFs.

MCCFs	Cage No.	Shape	Configuration	C_2 bond length (Å)[a]	Metal position[b]	Rotation	Ref.
$Sc_2C_2@C_{68}$	non-IPR C_{2v}(6073)	Butterfly	$[(Sc^{3+})_2(C_2)^{2-}]^{4+}$	(1.26)	Near [5,5] bond	C_2 rotating and oscillating	[18]
$Sc_2C_2@C_{72}$	non-IPR C_s(10528)	Butterfly	$[(Sc^{3+})_2(C_2)^{2-}]^{4+}$		Disordered	Metals jumping	[20]
$Sc_2C_2@C_{78}$	C_{2v}(24107)	Butterfly	$[(Sc^{3+})_2(C_2)^{2-}]^{4+}$	(1.27)	Near [6,6] bond		[21]
$Ti_2C_2@C_{78}$	D_{3h}(24109)	Linear	$[(Ti^{4+})_2(C_2)^{2-}]^{6+}$	(1.24)	Under 6MR	Fixed	[22,25]
$Zr_2C_2@C_{78}$	D_{3h}(24109)	Butterfly	$[(Zr^{4+})_2(C_2)^{2-}]^{6+}$	(1.28)	Under 6 MR	C_2 rotating	[25]
$Hf_2C_2@C_{78}$	D_{3h}(24109)	Zigzag	$[(Hf^{4+})_2(C_2)^{2-}]^{6+}$	(1.26)	Under 6 MR	C_2 rotating	[25]
$Sc_2C_2@C_{80}$	C_{2v}(31922)	Butterfly	$[(Sc^{3+})_2(C_2)^{2-}]^{4+}$	1.20	One under 6 MR, the other near [6,6] bond	Fixed	[26,55]
$Sc_3C_2@C_{80}$	I_h(31924)	Planar or trifoliate	$[(Sc^{3+})_3(C_2)^{3-}]^{6+}$	1.11	Disordered	Rotating	[27,28,96]
$Sc_4C_2@C_{80}$	I_h(31924)	Russian doll	$[(Sc^{3+})_4(C_2)^{6-}]^{6+}$	(1.48)		Rotating	[29,104]
$Sc_2C_2@C_{82}$(I)	C_s(39715)	Butterfly	$[(Sc^{3+})_2(C_2)^{2-}]^{4+}$	1.21	One under 6 MR, the other near [5,6,6] junction		[31,142]
$Sc_2C_2@C_{82}$(II)	C_{2v}(39718)	Butterfly	$[(Sc^{3+})_2(C_2)^{2-}]^{4+}$	1.18			[32]
$Sc_2C_2@C_{82}$(III)	C_{3v}(39717)	Butterfly	$[(Sc^{3+})_2(C_2)^{2-}]^{4+}$	1.19–1.20	Disordered	Oscillating	[55,124,125]
$Y_2C_2@C_{82}$ (I)	C_s(39715)	Butterfly	$[(Y^{3+})_2(C_2)^{2-}]^{4+}$				[34,37,142]
$Y_2C_2@C_{82}$ (II)	C_{2v}(39718)	Butterfly	$[(Y^{3+})_2(C_2)^{2-}]^{4+}$				[34]
$Y_2C_2@C_{82}$ (III)	C_{3v}(39717)	Butterfly	$[(Y^{3+})_2(C_2)^{2-}]^{4+}$	(1.27)	Along C_3 axis	Hopping	[33,34,37,127]
$Sc_2C_2@C_{84}$	D_{2d}(51591)	Butterfly	$[(Sc^{3+})_2(C_2)^{2-}]^{4+}$	1.20	Disordered	Rotating	[13,53,55]
$Y_2C_2@C_{84}$	non-IPR C_1(51383)	Butterfly	$[(Y^{3+})_2(C_2)^{2-}]^{4+}$		One under 6 MR, the other near [5,5] bond		[38]
$Gd_2C_2@C_{84}$	non-IPR C_1(51383)	Butterfly		1.23	one under 6 MR, the other near [5,5] bond		[39]
$Lu_3C_2@C_{88}$	D_2(81738)	Planar	$[(Lu^{3+})_3(C_2)^{3-}]^{6+}$	(1.30)		Oscillating	[41,103]
$Y_2C_2@C_{92}$	D_3(126408)	Zigzag	$[(Y^{3+})_2(C_2)^{2-}]^{4+}$	(1.27)		C_2 rotating	[37,42]
$Gd_2C_2@C_{92}$	D_3(126408)	Butterfly	$[(Gd^{3+})_2(C_2)^{2-}]^{4+}$	1.04	Disordered	Metals moving	[44]
$Y_2C_2@C_{100}$	D_5(285913)	Bias linear	$[(Y^{3+})_2(C_2)^{2-}]^{4+}$	(1.26)			[37]

[a] Computational results are given in parentheses.
[b] 5 and 6 denote pentagon and hexagon, respectively, 6MR and 5MR denote six-membered rings and five-membered rings.

In addition to the steric effect, the charge transfer from the cluster HOMOs to the cage LUMOs could shorten and elongate the bonds of the bonding and anti-bonding natures, respectively, and consequently lead to apparent cage distortion.

3.3. Electronic structure

Due to the intramolecular multielectron transfer from the carbides to the fullerene cages, the electronic structures of MCCFs can be formally described using an ionic model, $[(M^{3+,4+})_{2,3,4}(C_2)^{2-,3-,6-}]^{4+,6+}@C_{2n}{}^{4-,6-}$. The Group III or lanthanide and the Group IV metals present M^{3+} and M^{4+}, respectively, whereas the formal charge of a C_2 unit depends on its coordination type: μ_2-$C_2{}^{2-}$, μ_3-$C_2{}^{3-}$, or μ_4-$C_2{}^{6-}$ (Table 2). Therefore, a smaller number of electrons is expected to transfer from the metal carbide to the cages than the relevant pure metal clusters. The charge transfer generally leads to a stable closed-shell electronic configuration either for the carbon cage [94] or the whole MCCF [95].

The addition of electrons to a neutral empty fullerene changes the relative stability of the different isomers due to the alteration of the frontier orbital energy levels. As a result, the isomer favoring cluster incorporation is usually different from the most stable pristine fullerene. The filled orbitals include the LUMO to the LUMO + 2 and the LUMO to the LUMO + 1 for hexa-anionic and tetra-anionic cages, respectively. Accordingly, Poblet et al. proposed that free fullerene cages with large (LUMO + 3)–(LUMO + 2) [144] or (LUMO + 2)–(LUMO + 1) gaps [125] have considerable kinetic stability when encaging hexavalent or quadrivalent metal clusters. Despite being the least stable IPR isomer of C_{80}, I_h(31924)-C_{80} has a (LUMO + 3)–(LUMO + 2) gap as large as 1.86 eV [145], and thus is most stable when trapping metal clusters in the 6+ state [146]. Similarly, C_{3v}(39717)-C_{82} is very favorable for the $[M_2C_2]^{4+}$ (M = Sc, Y, and Er) encapsulations, although it is actually the highest in energy among the nine IPR C_{82} cages [125]. The marked stability stems from its unique (LUMO + 2)–(LUMO + 1) gap of greater than 1 eV among all IPR cages ranging from C_{60} to C_{100}. $Sc_2C_2@C_{3v}$(39717)-C_{82} remains the most abundant MCCF reported so far. Moreover, the molecular orbital rules have been validated in terms of excellent agreement between the computations and the XRD characterizations of the detailed molecular geometries, such as $Sc_2C_2@C_s$(39715)-C_{82} [31] and $Gd_2C_2@D_3$(126408)-C_{92} [44].

Theoretical calculations play an important role in the structural characterization when XRD data or NMR spectra are absent (due to low yield or poor solubility of the EMF samples). The number of fullerene isomers grows explosively as the cage size increases; thus, it is challenging for structure identification [48]. Unlike the case of empty cages, non-IPR isomers cannot be ruled out for EMFs due to the potentially enhanced stability caused by charge transfer. In practice, a feasible strategy is to first conduct semi-empirical calculations (e.g., AM1) for thousands of negatively charged (4- or 6-) cages; the screened low-energy cages are subsequently re-optimized in the endohedral forms at the higher levels to obtain their relative thermodynamic stabilities. A recent example is the theoretical determination of a Sc_2C_{80} isomer as $Sc_2C_2@C_{2v}$(24107)-C_{78} [21]. For non-IPR isomers, those holding fewer pentagon–pentagon fusions are preferential because of their lower local strains on the carbon skeletons [38]. Moreover, because the transferred electrons prefer to be added to the pentagons, cages with maximum pentagon separation often exhibit higher stability with decreased Coulomb repulsion [147].

3.4. Cluster–cage interplay

The cluster–cage interactions are dominated by metal–cage bonding. Hybrid, dative-bondings often form between metal ions and cages, whereas acetylide ions are mostly far from the

carbon skeletons, rendering weak C_2-cage interactions [125,148]. Metal–metal bonding is generally weak due to repulsive electrostatic interactions, whereas the bondings of metal–carbide carbons and the C_2 unit are much stronger [148]. The metal ions act as a mediator between the carbide carbons and the outer framework because there is no direct contact between the latter two.

The relative strengths between the cluster–cage and the intracluster interactions vary on a case-by-case basis. For example, covalent metal–cage and ionic metal–C_2 interactions were reported for Sc_3C_2@C_{80} [51] and Ti_2C_2@C_{78} [23]. In contrast, the Sc–C_2 distance (~1.96 Å) in Sc_4C_2@C_{80} is shorter than the Sc–cage distance (~2.20 Å), indicating a stronger covalent interaction between the Sc^{3+} cation and the C_2^{6-} anion [104]. The computed Sc–C_2 and Sc–cage distances for Sc_2C_2@C_{3v}-C_{82} are similar [125], which suggests strong covalent interaction between the Sc^{3+} cation and the C_2^{2-} anion.

The cluster and cage interact and stabilize mutually. Typically, linear Ti_2C_2 is unstable by itself and higher in energy than the butterfly configuration [149], but it is stabilized in D_{3h}-C_{78} [22]. Ti ions prefer to bind over hexagon rings and obtain most coordination in Ti_2C_2@C_{78}. The π-electron wave function in the HOMO-1 indicates considerable hybridization between C_{78}^{6-} and Ti^{4+} ions [74]. The good orbital symmetry matching (with respect to the σ_h plane of C_{78}) between the linear Ti_2C_2 cluster and the cage considerably lowers the molecular orbital energies of Ti_2C_2@C_{78} [22].

3.5. Effect of acetylide ion encapsulation

3.5.1. Bonding nature of the acetylide ion

In the early days, it was proposed that two carbon atoms prefer to be simultaneously encaged to avoid dangling bonds on the outer framework during cage shrinkage [66]. In most MCCFs, C_2 has a typical carbon–carbon triple bond length and is of a strong covalent nature [148] (Table 2). Despite the obvious shrinkage of the Y_2C_2 cluster, the C–C distances of 1.27 Å are maintained when the cage size gradually decreased from C_{100} down to C_{92}, C_{84}, and C_{82} [37]. Similar situations were found for the Sc_2C_2 cluster in D_{2d}(51591)-C_{84}, C_{3v}(39717)-C_{82}, and C_{2v}(31922)-C_{80}, where the C–C distances are all approximately 1.20 Å, regardless of cage size and symmetry [55]. The bond lengths of the C_2 unit are even intact after exohedral carbene addition to Sc_2C_2@C_{2v}(31922)-C_{80} [77]. C_2 appears to play a critical role in stabilizing the metal carbide cluster.

3.5.2. C_2 NMR chemical shift

It is difficult to detect ^{13}C NMR signals for the inner C_2 moiety [13,33,34]. The absence of the ^{13}C NMR peaks for the C_2 unit was previously interpreted in terms of considerable spin-rotation interaction: the lines were too broadened to be observed at room temperature [33,34].

However, one possible reason for these failures is that the C_2 signal is out of the typical measurement range. Compared with cage atoms, the computed chemical shifts for the C_2 unit are strongly deshielded in $[Sc_3C_2$@$C_{80}]^-$ and Sc_2C_2@C_{84} [51]. By using ^{13}C-enriched samples, Akasaka and co-workers first successfully detected chemical shifts for the carbide carbons of Sc_2C_2@C_{3v}(39717)-C_{82}, Sc_2C_2@D_{2d}(51591)-C_{84}, and $[Sc_3C_2$@I_h(31924)-$C_{80}]^-$ anion [50]. All the chemical shifts were observed in much lower fields (Table 3).

The local environments for the carbide carbons remained unaffected regardless of the outer framework. Dorn and co-workers reported improved ^{13}C NMR measurements for Y_2C_2@C_s(39715)-C_{82} and Y_2C_2@C_{3v}(39717)-C_{82}, in which similar chemical shifts for the inner C_2 were observed [37]. Thus, the shape and electronic environment of the $(Y_2C_2)^{4+}$ cluster may not change despite the cage symmetry difference between C_s- and C_{3v}–C_{82}. Similarly, the ^{13}C NMR signals of the C_2 unit in the pristine Sc_2C_2@C_{2v}(31922)-C_{80} are almost identical to the Ad derivatives (Table 3) [77].

Table 3
Observed chemical shifts (δ) for the carbide carbons in MCCFs and their derivatives.

Species	δ (ppm)	Ref.
Sc_2C_2@C_{2v}(31922)-C_{80}	231.5	[26]
Sc_2C_2@C_{2v}(31922)-C_{80}Ad	227.9/234.9/235.8/222.9[a]	[77]
$[Sc_3C_2$@I_h(31924)-$C_{80}]^-$	328.3	[50]
$[Sc_3C_2$@I_h(31924)-C_{80}Ad$]^-$	257.2, 384.4	[50]
Sc_2C_2@C_s(39715)-C_{82}	244.4	[31]
Sc_2C_2@C_{2v}(39718)-C_{82}	242.7	[32]
Sc_2C_2@C_{2v}(39718)-$C_{82}(CH_2)_2NCPh_3$	238.0	[32]
Sc_2C_2@C_{3v}(39717)-C_{82}	253.2	[50]
Y_2C_2@C_s(39715)-C_{82}	256.2	[37]
Y_2C_2@C_{3v}(39717)-C_{82}	257.0	[37]
Sc_2C_2@D_{2d}(51591)-C_{84}	249.2	[50]
Y_2C_2@C_1(51383)-C_{84}	247.8	[37]
Y_2C_2@D_3(126408)-C_{92}	227.3	[37]

[a] Chemical shift values of four mono-adduct isomers.

The carbide chemical shift has proven sensitive to the compression degree of the $(Y_2C_2)^{4+}$ cluster induced by the cage [37]. It gradually increases and becomes more deshielded from ~150 ppm for linear configuration to 227.3 ppm in C_{92}, 247.8 ppm in C_{84}, and reaches ~257 ppm in C_{82} cages (Table 3).

3.5.3. Effect of additional C_2: M_m@C_{2n} vs. M_mC_2@C_{2n}

The generation of an EMF may undergo a closed network formation pathway [150]. Starting from an M_m@C_{2n+2} precursor, a C_2 loss or encapsulation may lead to conventional M_m@C_{2n} or M_mC_2@C_{2n}, respectively [34]. The C_2 insertion considerably modifies the electronic structure of the M_m@C_{2n} and consequently affects its various properties. For example, the first oxidation potential of Sc_2C_2@C_{3v}(39717)-C_{82} (+0.47 V vs. Fc/Fc^+) is 420 mV higher than that of Sc_2@C_{3v}(39717)-C_{82} (+0.05 V vs. Fc/Fc^+) [78]. The change is attributed mainly to the much lower HOMO level of Sc_2C_2@C_{3v}(39717)-C_{82} than Sc_2@C_{3v}(39717)-C_{82}.

Compared with conventional EMFs, substantial changes in the UV and UPS are induced by the different number of electrons transferred from the metal–carbide clusters to the fullerene cages. Slight shifts of the UV peaks were observed by additional C_2 encapsulation to Y_2@C_{82} [33,34] or Er_2@C_{82} [36]. The onsets of Er_2@C_{82} (1820, 2420, 1600 nm for I, II, III, respectively) are all blue shifted in Er_2C_2@C_{82} (1550, 2400, 1250 nm for I, II, III, respectively), indicating larger HOMO–LUMO gap energies and therefore enhanced kinetic stabilities in the latter [36]. Furthermore, compared with Er_2@C_{82}, Er_2C_2@C_{82} (III) exhibits much stronger near-infrared photoluminescence (PL) at 1520 nm from the Er^{3+} ions. The phenomenon was attributed to its shifted onset (1250 nm), which reduced the possible absorbance of the C_{82} cage from PL of the encapsulated Er^{3+}.

In the UPS measurements, Y_2@C_{3v}(39717)-C_{82} and Y_2C_2@C_{3v}(39717)-C_{82} exhibited different spectral onset energies (0.45 eV vs. 0.8 eV) and peak positions (binding energies of the latter are ca. 0.2 eV lower than the former) [126]. These spectral features were rationalized by the two less electrons on the Y_2C_2@C_{3v}(39717)-C_{82} cage (formal charge transfer: Y_2@C_{82} 6 *e* vs. Y_2C_2@C_{82} 4 *e*). Likewise, the significant difference between Er_2@C_{3v}-C_{82} and Er_2C_2@C_{3v}-C_{82} in the UPS spectra also reflects their distinct electronic structures arising from the two excess electrons on the former cage [151].

3.6. Cluster motion

Like the conventional La_2@C_{80} [120,152] and Sc_3N@C_{80} [11], most MCCFs exhibit large cluster flexibility (Table 2). Some representatives are given below.

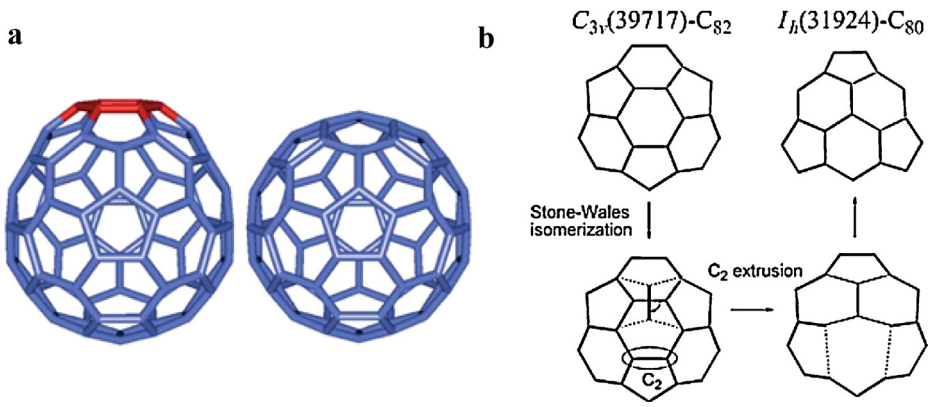

Fig. 20. (a) (left) The framework of C_{3v}(39717)-C_{82} structure. The 'cap' of six-membered ring is colored in red; (right) the framework of I_h-C_{80} structure from Ref. [33]. (b) the transformation from C_{3v}(39717)-C_{82} to I_h(31924)-C_{80}.
Adapted with permission from Ref. [125]. Copyright 2008 American Chemical Society (b).

We first focus on small cages, such as C_{68}, C_{72}, and C_{78}. It was proposed that the acetylide ion can freely rotate and oscillate between the Sc_2 unit in Sc_2C_2@C_{2v}(6073)-C_{68} at room temperature because the DFT computed energy barriers are as small as 0.7 and 2.2 kcal/mol [18]. The motion-induced equivalence of trapped atoms will lead to the observed symmetry of the outer cage in the ^{13}C NMR measurement. Therefore, the whole molecule exhibits C_{2v} symmetry and fulfills the observed 21 lines in the ^{13}C NMR spectrum.

For non-IPR EMFs, metal ions preferentially reside close to the adjacent pentagon pairs, and thus often present limited flexibility. In contrast, Feng et al. observed disordered Sc sites (both near and far from the fused pentagons) in the XRD structure of Sc_2C_2@C_s(10528)-C_{72}, indicating an unusual jumping motion inside this non-IPR cage [20].

Similar to Sc_2C_2@C_{68}, the C_2 unit in M_2C_2@C_{78} (M = Zr, Hf) may rapidly rotate around the long C_3 axis of the D_{3h}-C_{78} at room temperature due to the negligible energy barriers [25]. In contrast, the linear Ti_2C_2 is fixed in D_{3h}-C_{78}, and there exists a zigzag-cluster transition state structure between the linear and butterfly configurations with a high activation energy barrier (ca. 48.5 kcal/mol) [22].

Encapsulated in C_{80} cages, all of the Sc_mC_2 (m = 2, 3, 4) clusters possess motional behavior. Variable-temperature ^{13}C NMR spectrometry shows that the Sc_2C_2 cluster exhibits temperature-dependent dynamic motion in Sc_2C_2@C_{2v}(31922)-C_{80} [26]. At 298 K, the cluster was fixed with two nonequivalent Sc ions located on the mirror plane, and 41 lines [39 × 2 C; 2 × 1 C] were observed, in accordance with the C_s symmetry of the molecule. The hindrance of motion was reflected in the X-ray structure [55]. When heated to 413 K, the ^{13}C NMR spectrum pattern reduced to 22 lines [18 × 2 C; 4 × 1 C], completely reflecting the C_{2v} symmetry of the C_{80} cage. The ^{45}Sc NMR spectra show that two lines of equal intensity separated by 30 ppm at 293 K coalesce into one peak at temperatures higher than 353 K. Thus, the Sc atoms become equal due to the rapid Sc_2C_2 rotation.

Compared with the temperature-dependent behavior of Sc_2C_2@C_{2v}(31922)-C_{80}, the free motions of the larger Sc_3C_2 and Sc_4C_2 in I_h-C_{80} were observed at room temperature. The symmetric hyperfine splitting of 22 lines in early ESR/EPR observations suggested three magnetically equivalent ^{45}Sc atoms in paramagnetic Sc_3C_2@I_h-C_{80} at room temperature [76,79,81–83,86–88]. Temperature dependent behavior in ESR spectra was also reported for Sc_3C_2@C_{80} [86]. MEM analysis suggested that the Sc_3C_2 cluster is disordered with five directions in the cyclacene-like belt of C_{80}, implying a free hopping along the belt [28]. More convincingly, ^{13}C NMR measurement showed two lines for both of them, which is only reasonable for an icosahedral I_h-C_{80} with rapidly rotating clusters inside [27,104].

Theoretical calculations shed more lights on the cluster motions. DFT study found that different isomers of Sc_3C_2@C_{80} have very small energy differences (<10 kcal/mol), indicating large flexibility of the Sc_3C_2 cluster inside I_h-C_{80} [96]. The cluster can change between a planar and trifoliate shape due to the smooth potential energy surface [27]. The first principles molecular dynamics simulations revealed a slightly complex motion scenario in Sc_3C_2@C_{80}:Sc_3 trimer ratchets along the equatorial belt of the six-membered rings on the I_h-C_{80} cage with rapid C_2 flipping through the Sc_3 plane [51]. By overcoming a small rotation barrier (2.8 kcal/mol), the Sc_4C_2 moiety can rotate freely around the C_2 axis of I_h-C_{80} [104], whereas the C_2 unit may migrate in the Sc_4C_2@C_{80} [105]. The free cluster motions are consistent with the computed flat concentric circles of the electrostatic potential map inside I_h-C_{80}^{6-} [120].

C_{3v}(39717)-C_{82} has a carbon skeleton analogous to I_h-C_{80} and a rather spacious interior to accommodate metal clusters (Fig. 20a). One can obtain an I_h-C_{80} from a C_{3v}(39717)-C_{82} by a Stone-Wales isomerization followed by a C_2 extrusion on the cap shown in Fig. 20b [125]. Similar to I_h-C_{80}, the computed electrostatic potential map inside C_{3v}(39717)-C_{82}^{6-} exhibits smooth concentric circles around the C_3 axis, very favorable for cluster rotation [93].

Hulman et al. observed temperature-dependent behavior for two lines (721 and 734 cm^{-1}) in the IR spectrum of Sc_2C_2@C_{3v}(39717)-C_{82} above 200 K, suggesting triggered molecular motion at higher temperature [115]. However, they could not identify which moiety, cage or entrapped metals accounted for the phenomenon at that time. The inner C_2 moiety rotation in Sc_2C_2@C_{3v}(39717)-C_{82} was proposed by observing its ^{13}C NMR line broadening when the temperature increased from 253 to 303 K [50]. MEM analysis suggested that the scandium atoms may hop along the trajectory connecting the center of six-membered rings in Sc_2C_2@C_{3v}(39717)-C_{82} [123]. The motion was supported by DFT calculations: the largest energy difference is only 5.2 kcal/mol for various Sc_2C_2@C_{3v}(39717)-C_{82} isomers featuring different cluster orientations inside the cage [125].

More solid experimental evidence comes from the ^{13}C NMR and X-ray single-crystal analysis. The observed ^{13}C NMR lines only originate from the C_{3v}(39717)-C_{82} cage or its Ad derivative [30,124]. Moreover, there are three pairs of Sc sites at different positions in either Sc_2C_2@C_{3v}(39717)-C_{82}(Ad) [124] or Sc_2C_2@C_{3v}(39717)-C_{82}·Co(OEP)·2$CHCl_3$ crystal systems [55], indicating oscillating motion of the cluster inside the cage.

Consistent with the above results, the ^{45}Sc NMR spectra show one signal for Sc_2C_2@C_{3v}(39717)-C_{82} but two lines for

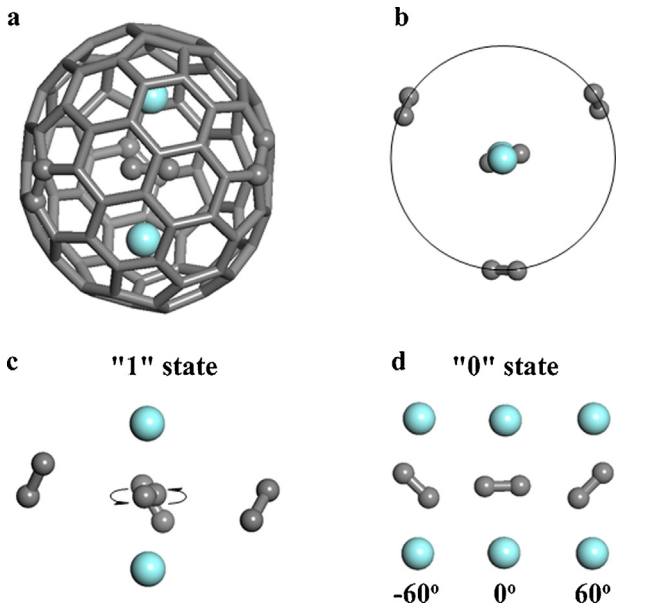

Fig. 21. (a) $Y_2C_2@D_3(126408)$-C_{92} with planar Y_2C_2 unit. (b) Top view of the C_2 rotation plane. (c) "1" state; all C_2 rotations about the Y_2 axis remain parallel to the C_2 rotation plane due to an applied voltage (100 meV) which removes the effect of the rotational barrier. (d) "0" state; C_2 rotations about the Y_2 axis alternate between three states, −60°, 0°, and 60°, which tunnel through the C_2 rotation plane due to the rotational barrier from Ref. [42].

$Sc_2C_2@C_s(39715)$-C_{82}, indicating non-equivalent Sc ions inside the $C_s(39715)$-C_{82} at room temperature [31,114,124]. However, the two signals gradually merged when increasing the temperature and finally exhibited only one line above 373 K. This phenomenon was attributed to rapid Sc_2 rotation at higher temperature, which caused equivalent magnetic environments for the two metals.

Similar to Sc_2C_2, the motion of the Y_2C_2 cluster in $C_{3v}(39717)$-C_{82} was elucidated both experimentally and theoretically. Previous electron density distribution analysis implied no direct covalent bonds between Y_2 and $C_{3v}(39717)$-C_{82}; therefore, the cluster may rotate around the C_3 axis of the cage [128]. MEM/Rietveld analysis revealed that the hopping of the Y–Y ion pair around the C_2 center forms the pentagonal–dodecahedral charge density in $Y_2C_2@C_{3v}(39717)$-C_{82} [127]. The Y_2C_2 unit can rotate around the C_3 axis in $Y_2C_2@C_{3v}(39717)$-C_{82} to satisfy the observed C_{3v} cage symmetry [33].

For crystalline $Sc_2C_2@D_{2d}(51591)$-C_{84}, previous low energy Raman scattering spectra disclosed that the diatomic C_2 unit can rotate in a plane perpendicular to the long C_2 axis of C_{84} and form a planar quantum rotor with an energy barrier as small as a few meV [53]. The quantized rotational state of the Sc_2C_2 cluster may couple with the classical rotational motion of the C_{84} cage [153]. DFT calculations suggested that the planar Sc_2C_2 unit can only rotate around the Sc–Sc axis and not around the whole cage [54]. The respective rotation behaviors of the Sc and C atoms were definitively demonstrated by the four pairs of sites for Sc atoms and the three positions for the C_2 unit observed in its X-ray structures [55]. A comparison of the degree of disorder for the Sc_2C_2 in the X-ray data of $Sc_2C_2@C_{2v}(31922)$-C_{80}, $Sc_2C_2@C_{3v}(39717)$-C_{82}, and $Sc_2C_2@D_{2d}(51591)$-C_{84} revealed that the metal cluster has more and more flexibility as the cage size increases [55]. The cage volume plays a crucial role in dictating the cluster motion.

DFT computations and Raman spectroscopic analysis revealed that the C_2 in $Y_2C_2@D_3(126408)$-C_{92} may rotate around the line connecting the two Y atoms and tunnel through the C_2 rotation plane (i.e., alternate one C up and the other down; Fig. 21) [37,42]. The whole Y_2C_2 cluster acts as a carousel, and its rotation

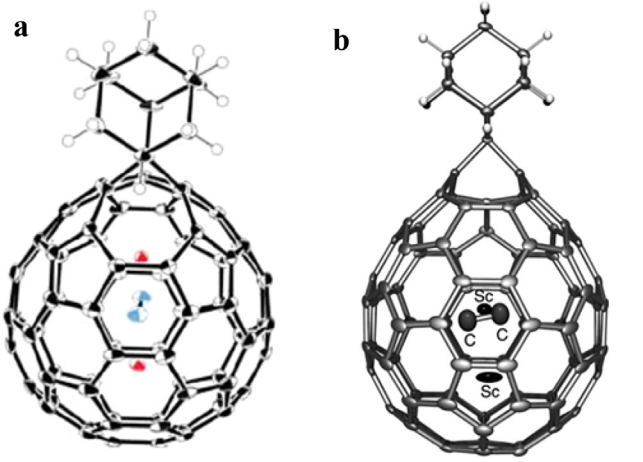

Fig. 22. ORTEP drawings of (a) $Sc_2C_2@C_{2v}(31922)$-C_{80}(Ad) from Ref. [26] and (b) $Sc_2C_2@C_{3v}(39717)$-C_{82}(Ad) with thermal ellipsoids shown at the 50% probability level from Ref. [124].

is hampered at low temperature due to the enhanced cluster–cage interactions. Unlike the in-plane rotation in $Sc_2C_2@C_{84}$, the C_2 unit of Y_2C_2 undergoes three orientations, two zigzag (±60°) and one plane butterfly (0°) ("0" state in Fig. 21) with an energy difference of 79.3 meV. The C_2 will stop tunneling ("1" state) when a small voltage (100 meV) is applied to the cage to overcome the rotational barrier. This voltage-controlled state transition may find applications in memory devices and quantum computers.

The multiple occupancy sites observed for the Gd ions in the $Gd_2C_2@D_3(126408)$-C_{92} crystal indicate that they are flexible to move about the inner cage surface [44]. The motion may be reflected by 20–100 cm^{-1} broadening in the low-energy Raman spectroscopy [43].

4. Exohedral reactivity

Exohedral functionalization is essential to improve the solubility and accessibility of EMFs for practical applications. One alluring aspect is that the position and motion of encaged species become controllable by exohedral functionalization. For example, when electron-donating molecules (such as disilirane) are attached, the free rotations of the two metal atoms in $La_2@C_{80}$ and $Ce_2@C_{80}$ are restricted to circular motion in a plane and are almost fixed, respectively [154,155]. In addition, the electronic and paramagnetic properties of EMFs can be finely adjusted upon chemical modification, and the derivatives can bear novel properties never expected for pristine EMFs.

The chemical properties of MCCFs are rarely reported, most likely due to their lower yield compared to classical and TNT EMFs. The first MCCF reaction is Ad addition on $Sc_3C_2@C_{80}$ [27]. X-ray data showed that the reaction occurred at a [6,6] junction (Fig. 8b), and the whole $Sc_3C_2@C_{80}$(Ad) molecule exhibited C_s symmetry. The paramagnetic properties of $Sc_3C_2@C_{80}$ can be tuned by chemical modifications, such as carbene addition. In contrast to the 22 lines for pristine $Sc_3C_2@C_{80}$, the ESR spectrum for the two isomers of its Ad cycloadducts presents 15 lines split into 8, indicating that the C_{3v} symmetry of the Sc trimer in $Sc_3C_2@C_{80}$ is reduced to C_{2v} upon chemical functionalization [156]. The large cluster flexibility in $Sc_3C_2@C_{80}$ might also be modulated by exohedral Ad addition. The line width decreases by the factor of 2 upon chemical functionalization, suggesting hindered inner rotation in the carbene adducts. The Ad group selectively attacks a [6,6] junction of $Sc_2C_2@C_{2v}(31922)$-C_{80} to form the mono-adduct (Fig. 22a), which leads to an open-cage local geometry near one Sc ion [26]. The much lower onset of

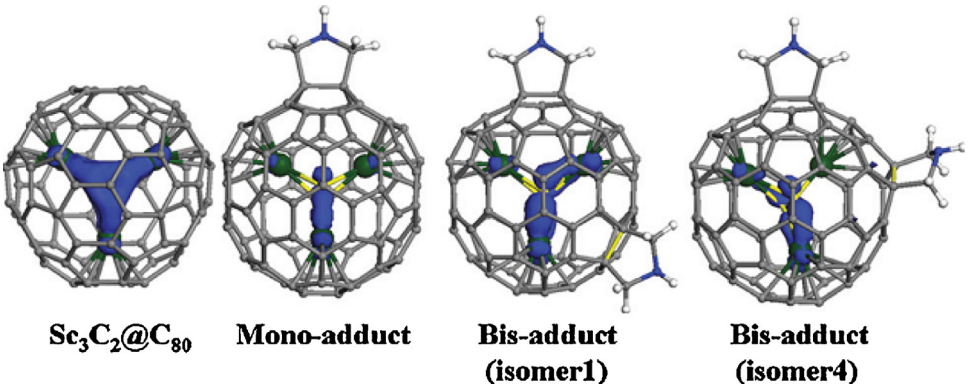

Fig. 23. The calculated spin density distributions of $Sc_3C_2@C_{80}$ and its fulleropyrrolidines. The blue area presents the unpaired spin. Reproduced from Ref. [159] with permission of The Royal Society of Chemistry.

$Sc_2C_2@C_{2v}(31922)$-C_{80} in the UV–vis–NIR spectrum indicates a small gap and high chemical reactivity [47]. The photochemical reactions between $Sc_2C_2@C_{2v}(31922)$-C_{80} and 2-adamantane-2,3-[3*H*]-diazirine (AdN_2) yield five stable Ad monoadducts [77]. In comparison, the formation of $Sc_2C_2@C_{3v}(39717)$-C_{82}(Ad) occurs at a [5,6] junction with an open-cage structure (Fig. 22b) [124].

Lu et al. first reported the 1,3-dipolar cycloaddition reaction of $Sc_2C_2@C_s(39715)$-C_{82} [31]. Typically, a mixture of 5 mg of $Sc_2C_2@C_s(39715)$-C_{82} and an excess amount (ca. 30-fold) of 3-triphenylmethyl-5-oxazolidinone was heated in 40 ml of a toluene/ODCD solution under reflux in an argon atmosphere. The obtained product was subjected to crystal growth at 253 K for structural characterization. Fig. 12 depicts the X-ray structure of the major enantiomer of the $Sc_2C_2@C_s(39715)$-$C_{82}(CH_2)_2$NTrt (Trt = triphenylmethyl) monoadduct. The addition selectively occurs at a [6,6] junction far from the butterfly-shaped Sc_2C_2 cluster, and the carbon framework near the pyrrolidino ring remains closed. The regioselectivity can be partially rationalized by frontier molecular orbital theory: the LUMO is mainly contributed by the cage carbons far from the cluster, and they are thus favorable to 1,3-dipolar addition. The same 1,3-dipolar reaction for $Sc_2C_2@C_{2v}(39718)$-C_{82} affords three monoadduct isomers, **A**, **B**, and **C**, with a relative ratio of 2:1.5:1 [32]. Their LUMO distributions suggest that the reaction sites are the [5,6], [6,6], and [6,6] junctions, respectively, and the addition pattern of isomer **A** has been confirmed by X-ray single-crystal data (Fig. 12). The chemical modification drastically altered the electronic and electrochemical properties of $Sc_2C_2@C_{82}$. Most of the redox potentials of $Sc_2C_2@C_s(39715)$-C_{82} are cathodically shifted by 0.1–0.3 V, whereas the UV-vis NIR spectra lines are blue shifted. For $Sc_2C_2@C_{2v}(39718)$-C_{82}, its electrochemical bandgap (0.99 V) is markedly enlarged upon exohedral functionalization (**A**: 1.40 V; **B**: 1.23 V; **C**: 1.19 V).

Similarly, Wang et al. synthesized and isolated a $Sc_3C_2@C_{80}$ fulleropyrrolidine mono-adduct via the Prato reaction (Fig. 23) [157]. It was suggested that the addition occurred at the [5,6] junction of the C_{80} cage, based on the non-equivalent methylene protons and the equivalent methylene carbon atoms observed in the ^{13}C NMR and heteronuclear multiple quantum coherence (HMQC) spectra. The obvious regioselectivity is in line with the latest theoretical study [158]. In contrast to the single peak at 670 cm^{-1} in the FTIR spectra for the pristine $Sc_3C_2@C_{80}$, the antisymmetric Sc–C stretching vibrations mode for the fulleropyrrolidine adduct appeared at approximately 693 and 714 cm^{-1}. This phenomenon was attributed to the deformed Sc_3C_2 configuration upon exohedral addition. According to their DFT calculations, the symmetry of the Sc_3C_2 clusters reduces from the original C_{3v} in $Sc_3C_2@C_{80}$ to C_{2v} in the monoadduct (Fig. 23). Simultaneously, compared to homogeneous distribution on the three Sc atoms in $Sc_3C_2@C_{80}$, a higher spin density prefers to be localized on the Sc atoms far from the pyrrolidine addend (Fig. 23). Following the mono-adduct, they further prepared and isolated nine $Sc_3C_2@C_{80}$ fulleropyrrolidine bis-adducts [159]. Depending on the addition sites of the second pyrrolidine, the bis-adducts exhibited diverse unpaired spin distributions on the endocluster (Fig. 23). The spin divergence of mono- and bis-adducts directly caused their differences in the ESR spectra

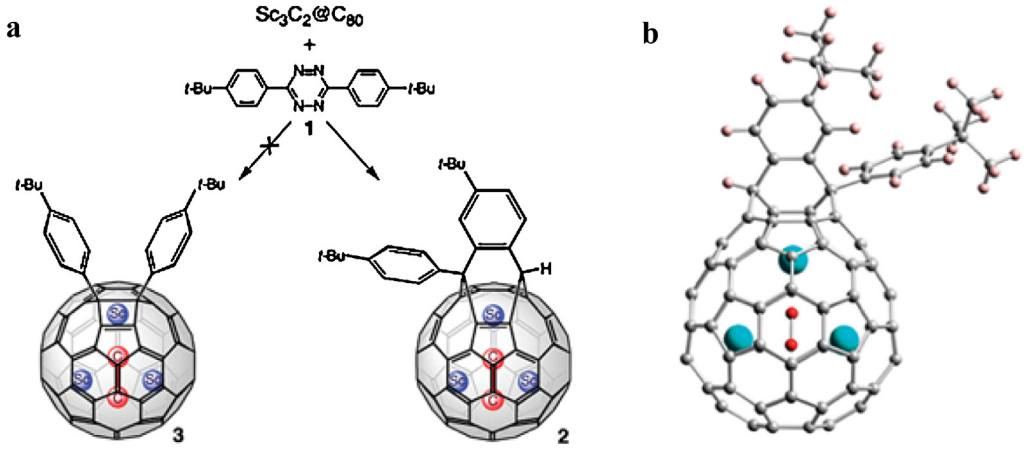

Fig. 24. (a) Reaction of tetrazine **1** with $Sc_3C_2@C_{80}$ giving bisfulleroid **2** instead of the expected four-membered ring product **3**. (b) Optimized structure of **2**. Adapted with permission from Ref. [160]. Copyright 2012 American Chemical Society.

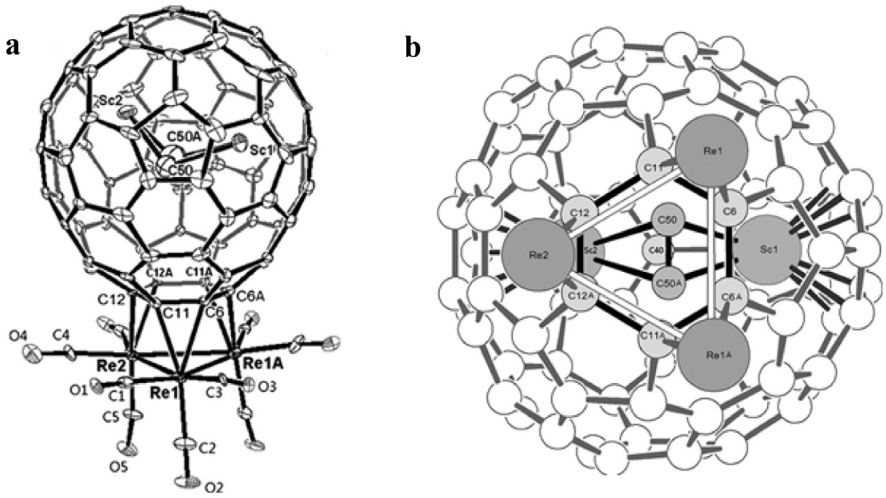

Fig. 25. (a) Molecular structure of $[(\mu\text{-H})_3Re_3(CO)_9\text{-}(\eta^2, \eta^2, \eta^2\text{-}Sc_2C_2@C_{3v}(39717)\text{-}C_{82})]$. Thermal elliposids are shown at 30% probability. The Re atoms and the Sc_2C_2 moiety are disordered at their sites; the ORTEP diagram displays the Re atoms with 95% and the C_2Sc_2 moiety with 50% occupancy. (b) Highlighted configuration. A plane of symmetry passes through the Re2, Sc2, C40, and Sc1 atoms.

Reprinted with permission from Ref. [161]. Copyright Wiley-VCH 2012.

compared to the pristine $Sc_3C_2@C_{80}$. The authors believed that controllable paramagnetism induced by exohedral functionalization is significant for the design of novel molecular devices.

Kurihara et al. studied the reaction between $Sc_3C_2@C_{80}$ and a substituted tetrazine **1**, which was expected to afford a C_2-inserted product **3** (Fig. 24a) [160]. To their surprise, a bisfulleroid **2** derivative holding a doubly bridged 14-membered ring was obtained. NMR measurements combined with theoretical simulations suggested that the open-cage addition occurred at the [5,6] junction (Fig. 24b). The EPR spectra of **2** exhibit two sets of hfcc at 6.73 G (one Sc nucleus) and 4.00 G (two Sc nuclei). Thus, although the addend can induce the cage expansion and trap one Sc atom in the formed bisfulleroid bulge, the other two Sc atoms can still rotate around the cage to become equivalent.

Coordination chemistry of EMFs lags behind their standard chemical functionlizations. Chen et al. recently reported an $Sc_2C_2@C_{3v}(39717)\text{-}C_{82}$ complexation with a Re_3 cluster [161]. Briefly, pure $Sc_2C_2@C_{3v}(39717)\text{-}C_{82}$ sample was synthesized and treated with $[(\mu\text{-H})_3Re_3(CO)_{11}\text{-(NCMe)}]$ in chlorobenzene for 3.5 h, followed by HPLC purification and recrystallization, and finally an air-stable $[(\mu\text{-H})_3Re_3(CO)_9\text{-}(\eta^2, \eta^2, \eta^2\text{-}Sc_2C_2@C_{3v}(39717)\text{-}C_{82})]$ solid was achieved. The XRD data shows that the addition occurred at the unique hexagon ring of the $C_{3v}(39717)\text{-}C_{82}$ surrounded by three pentagons and three hexagons in a highly regioselective manner (Fig. 25). The Re_3 triangle is nearly parallel to the protruding hexagon plane. Although the complexation left the Sc_2C_2 cluster almost intact, an elongated Sc–C distance (2.40 Å) compared to the pristine $Sc_2C_2@C_{3v}(39717)\text{-}C_{82}$ (2.21 Å) was observed. The authors suggested that this phenomenon may be due to the deformed C_{82} framework and different charge distribution upon Re_3 cluster coordination.

The interaction between the inner cluster and the outer cage affects the chemical reactivity of a clusterfullerene. Theoretical studies can help disclose the reaction rules and interpret the experimental observations [3i]. Comprehensive DFT calculations on the Diels–Alder cycloaddition between 1,3-butadiene and $Ti_2C_2@D_{3h}(24109)\text{-}C_{78}$ revealed that the cluster encapsulation significantly modifies both the reactivity and the regioselectivity of the C_{78} fullerene [143]. Certain types of unreactive bonds are activated, and some are deactivated, with the whole reaction energies reduced relative to the hollow cage. The change was primarily attributed to the structural deformation of the carbon framework and the alteration of its LUMOs upon Ti_2C_2 insertion.

Moreover, the nature of the endohedral composition can tune the chemical reactivity. For example, despite having the same $C_s(39715)\text{-}C_{82}$ cage, $Y_2C_2@C_s\text{-}C_{82}$ is favorable for the Bingel–Hirsch reaction and yields derivatives in 20 min at 273 K, whereas $Sc_2C_2@C_s\text{-}C_{82}$ needs 2 h at 293 K to afford the corresponding monoadducts [142]. The reactivity difference could be explained by their diverse LUMO distributions: the LUMO of $Y_2C_2@C_s\text{-}C_{82}$ is mainly contributed by the cage, whereas that of $Sc_2C_2@C_s\text{-}C_{82}$ is localized on both the cage and the Sc metals.

5. Properties and potential applications

5.1. Electrochemical properties

Table 4 summarizes the redox potentials of the MCCFs measured so far. Except for the open-shell $Sc_3C_2@C_{80}$, all the MCCFs exhibit high first redox potentials and wide electrochemical gaps $\geq$1.0 V. Note that exohedral modification alters the electrochemical properties of an MCCF such as $Sc_2C_2@C_{2v}(31922)\text{-}C_{80}$ [77].

Table 4
Reported redox potentials (V vs. Fc/Fc^+) and electrochemical gaps of MCCFs.

MCCFs	$^{ox}E_2$	$^{ox}E_1$	$^{red}E_1$	$^{red}E_2$	$^{red}E_3$	ΔE ($^{ox}E_1$–$^{red}E_1$)	Ref.
$Sc_2C_2@C_s(10528)\text{-}C_{72}$		0.41	−1.19	−1.54	−1.75	1.60	[20]
$Sc_2C_2@C_{2v}(31922)\text{-}C_{80}$		0.41	−0.74	−1.33		1.15	[77]
$Sc_3C_2@I_h(31924)\text{-}C_{80}$		−0.03	−0.50	−1.64	−1.84	0.47	[90]
$Sc_4C_2@I_h(31924)\text{-}C_{80}$	1.10	0.40	−1.16	−1.65		1.56	[29]
$Sc_2C_2@C_s(39715)\text{-}C_{82}$	0.64	0.42	−0.93	−1.30		1.35	[31]
$Sc_2C_2@C_{2v}(39718)\text{-}C_{82}$	0.67	0.25	−0.74	−0.96		0.99	[32]
$Sc_2C_2@C_{3v}(39717)\text{-}C_{82}$		0.47	−0.94			1.41	[124]
$Lu_3C_2@D_2(81738)\text{-}C_{88}$		0.31	−1.34	−1.70	−2.15	1.65	[41]

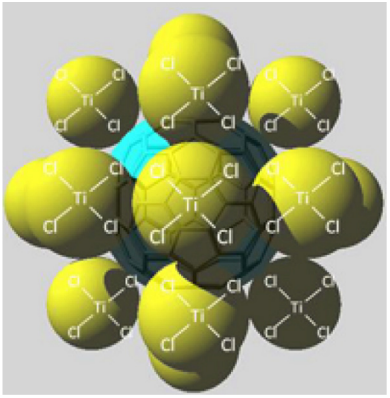

Fig. 26. Schematic view of metallofullerene complexation with $TiCl_4$. The centered light blue sphere and surrounding yellow spheres represent metallofullerene and $TiCl_4$, respectively.

Reprinted with permission from Ref. [162]. Copyright 2012 American Chemical Society.

Since their discovery, low production yield and tedious HPLC separation have hindered EMFs research. Such experimental difficulties are sometimes responsible for the erroneous assignment of MCCFs as classical EMFs. Shinohara and co-workers recently demonstrated that $TiCl_4$ Lewis acid can be employed to effectively and quickly separate and purify diverse classical and carbide EMFs from empty fullerenes in a few minutes [162]. All the EMFs featuring a first oxidation potential $^{ox}E_1$ lower than 0.5 to 0.6 V vs. Fc/Fc^+ might react with $TiCl_4$ to afford stable complexes (Fig. 26) and become highly purified (>99%). The $^{ox}E_1$ threshold was adjusted to 0.62–0.72 V vs. Fc/Fc^+ in a later report [163]. All the $^{ox}E_1$ values for MCCFs reported so far meet this requirement and can be separated efficiently (Table 4). This method may replace the conventional HPLC technique and promises a bright future for the high-efficiency isolation of MCCFs.

5.2. Magnetic properties

The achievement of the electron spin manipulation of EMFs is crucial for their potential application in quantum information processing. Ma et al. prepared $Y_2@C_s$-C_{82}, $Y_2C_2@C_s$-C_{82}, $Sc_2C_2@C_s$-C_{82} anions and observed diverse features in their ESR spectra (Fig. 27) [142]. They argued that these discrepancies stemmed from the different LUMO distributions on the three molecules and concluded that electron spin can be altered by the C_2 encapsulation into the same C_s-C_{82} cage and can be finely adjusted by changing the metal species in the MCCFs. The stable and controllable electron spins render these MCCF anion radicals promising materials in the field of quantum computing.

A synchrotron soft X-ray magnetic circular dichroism (SXMCD) study on $Er_2C_2@C_{2v}$-C_{82} performed by Shinohara and coworkers revealed paramagnetic behavior in sharp contrast to the strong antiferromagnetic-like characteristics of $Er@C_{2v}$-C_{82} [35]. The high magnetic susceptibility was explained in terms of the closed-shell carbon framework after accepting 6 *e* from the Er atoms, which hinders the intermolecular antiferromagnetic-like interactions between neighboring C_{82} cages. Moreover, the SXMCD results indicated that effective magnetic moments can be tuned by changing the cage symmetry from C_{2v}-C_{82} to C_s-C_{82}. Hetero $ErYC_2@C_s$-C_{82}, which processes both paramagnetic Er^{3+} and diamagnetic Y^{3+} ions, exhibits similar magnetic susceptibility to $Er_2C_2@C_s$-C_{82}, suggesting negligible substitution effects on the Er^{3+} electronic state [35].

After reduction by potassium metal in THF solution, $Sc_3NC@C_{80}$ becomes a stable paramagnetic anion radical $Sc_3NC@C_{80}^{\bullet-}$ and

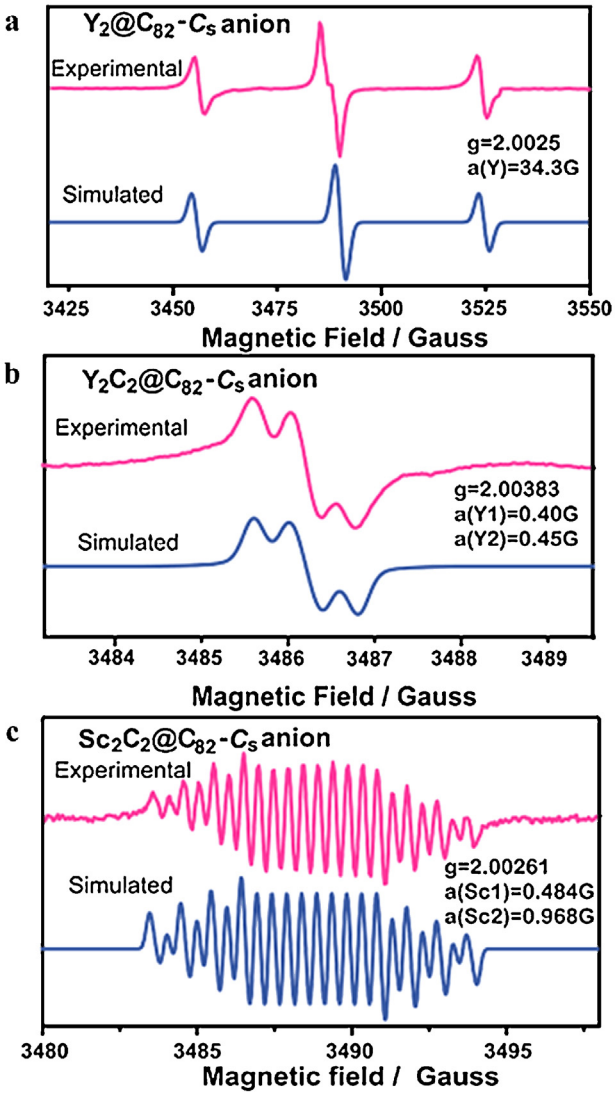

Fig. 27. The experimental and simulated ESR spectra of (a) $Y_2@C_s$-C_{82}, (b) $Y_2C_2@C_s$-C_{82}, and (c) $Sc_2C_2@C_s$-C_{82} anion radicals.

Adapted with permission from Ref. [142]. Copyright 2013 American Chemical Society.

exhibits 36 symmetric lines in ESR spectrometry [134]. DFT calculations indicate that the LUMO of neutral $Sc_3NC@C_{80}$ is mainly contributed by the NC moiety, which possesses the unpaired electron, and the large spin density in the anion. Accordingly, the electronic structure changes from $(Sc^{3+})_3(NC)^{3-}@C_{80}^{6-}$ to $(Sc^{3+})_3(NC)^{4-}@C_{80}^{6-}$ upon reduction. The NC unit plays a critical role in the stability of this paramagnetic radical. The authors argued that this was the first realization of a spin-active paramagnetic species for metal cyanide EMFs.

5.3. Electronic transport properties

$Sc_3C_2@C_{80}$ crystal is an n-type semiconductor with a small computed band gap (0.07 eV). The time-resolved microwave conductivity measurements found that its thin film presents an electron mobility ($\mu = 0.13\ cm^2\ V^{-1}\ s^{-1}$) 2 orders of magnitude higher than $La_2@C_{80}$ and $Sc_3N@C_{80}$, although they all have the same I_h-C_{80} outer cage [164]. The good charge-transport ability was attributed to the paramagnetic nature and small band gap of $Sc_3C_2@C_{80}$, which facilitate the valence electrons excitation to the conduction bands to generate electron and hole carriers. Thus,

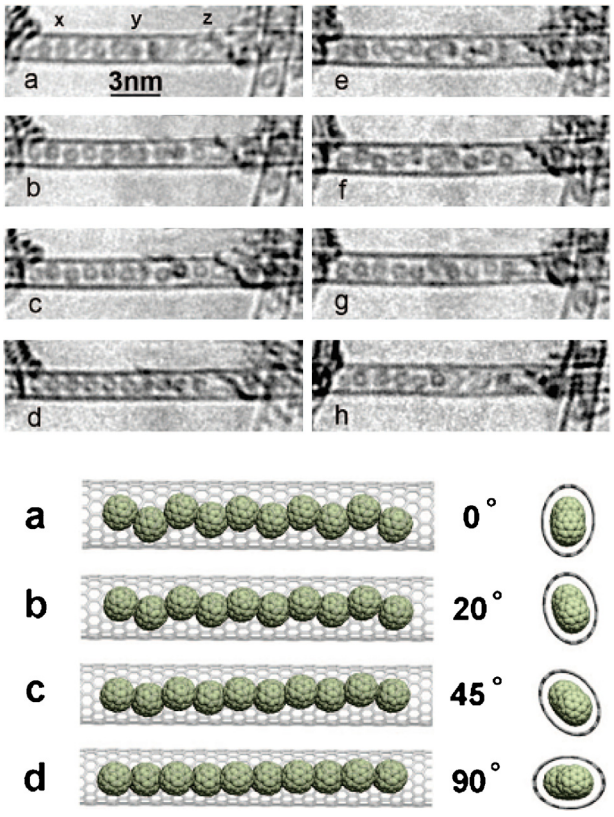

Fig. 28. (upper panel) TEM images of $Sc_3C_2@I_h$-C_{80} SWNT peapods as a function of time. (a–h). Each image has 2 s acquisition and 10 s between frames. (Lower panel) Schematic representation of the rotation of a zigzag chain of $Sc_3C_2@I_h$-C_{80} inside a SWNT causing structural deformation that leads to an elliptical cross section.
Adapted with permission from Ref. [167]. Copyright 2008 American Chemical Society.

$Sc_3C_2@C_{80}$ is a promising candidate for the design of novel electronic devices.

5.4. Potential applications

Gadolinium-containing MCCFs, $Gd_2C_2@C_{84}$ and $Gd_2C_2@C_{92}$, in their water-soluble forms may contribute to the development of second-generation relaxation agents for magnetic resonance imaging (MRI) [165]. Likewise, lutetium-based MCCFs, such as $Lu_3C_2@C_{88}$, may serve as multifunctional contrast agents for X-ray, MRI, and radiopharmaceuticals due to the high absorptivity of the Lu atoms [166].

The flexible motions of the metal carbide clusters inside the fullerene cages may lead to potential use of the MCCFs as molecular devices. For example, the temperature-dependent cluster motions alter the symmetry of $Sc_2C_2@C_{80}$ (C_s and C_{2v} at low and high temperature, respectively), which renders this MCCF a useful molecular thermometer [26]. Featuring a C_2 rotor, $Sc_2C_2@C_{84}$ [53] and $Y_2C_2@C_{92}$ [42], together with the nesting Russian-doll $Sc_4C_2@C_{80}$ [29,104], may find application in quantum information processing.

In addition, the encapsulation of MCCFs into nanotubes can create hybrid nanomaterials, i.e., peapods, which exhibit intriguing functional characteristics. Warner et al. observed in their TEM experiments that $Sc_3C_2@I_h$-C_{80} molecules assumed a zigzag packing structure to coalesce into 10 nm long chains, which slowly rotated inside single-walled carbon nanotubes (SWNTs) (Fig. 28) [167]. Along with the rotation, the diameter of the SWNTs expanded and contracted in turn. The authors attributed this phenomenon to the higher HOMO energy level and smaller ionization potential of $Sc_3C_2@I_h$-C_{80} compared to conventional fullerenes, which facilitate its ionization under electron beam irradiation. To minimize Coulomb repulsions, a zigzag packing arrangement is favored for the inner charged cages, which subsequently induces strain on the SWNT and deforms its cross section. Accordingly, it was suggested that the $Sc_3C_2@I_h$-C_{80} peapods might hold potential application for nanoactuation. In addition, Iijima et al. demonstrated that the local DOS of SWNTs can be modulated by encapsulating both $Pr@C_{82}$ and $Sc_3C_2@C_{80}$ simultaneously [168].

On the other hand, MCCFs such as $Sc_3C_2@C_{80}$ [27] and $Lu_3C_2@C_{88}$ [41] hold unusual open-shell electronic configurations; their paramagnetisms can be finely tuned by exohedral functionalization [157,159] and have potential applications in magnetic materials. For $Er_2C_2@C_{82}$, the enhanced near-infrared photoluminescence at 1520 nm from the Er^{3+} ions promises possible application in designing novel optical materials [36]. The successful fabrication of its ordered two-dimensional layer structure paved the way toward future nanoapplication of this MCCF molecule [169].

6. Concluding remarks

Tremendous efforts have been devoted to MCCFs during the last decade; however, this novel branch of the EMFs is still in its infancy, and many plausible members have not been conclusively identified to date. For instance, in the early gas-phase ion mobility measurements of various Sc-containing EMFs, Shinohara and co-workers detected two cage sizes (C_n^+ and C_{n-2}^+) for most $Sc_2C_n^+$ ($n \leq 86$), and only the smaller size for the larger ones ($n \geq 88$) [66]. The smaller cages might correspond to carbide metallofullerenes. Three Ti_2C_{84} isomers were previously isolated and characterized by mass spectrometry, UV–vis–NIR, and EELS spectroscopy [170]. It is likely that new MCCFs will be found in the form of $Ti_2C_2@C_{82}$. Shinohara and coworkers recently reported a linear relationship between the effective volume and the number of carbon atoms of the EMFs [171]. Based on this finding, they suggested many probable MCCFs, including $Sc_2C_2@C_{72}$ (confirmed in Ref. [20]), $Sc_2C_2@C_{74}$, $Sc_2C_2@C_{76}$, $Ti_2C_2@C_{82}$(II, III), $Y_2C_2@C_{80}$(II), $Lu_2C_2@C_{72}$, $Lu_2C_2@C_{74}$(I), $Lu_2C_2@C_{80}$, and $Lu_2C_2@C_{82}$(III).

There are many more examples regarding other metal elements. Yang et al. detected a series of mass spectrum signals for digadolinium endohedrals with cage sizes ranging from C_{90} to C_{124}; only a few were subjected to further characterization [44]. In addition to the already confirmed $Gd_2C_2@D_3(126408)$-C_{92}, more MCCFs, such as $Gd_2C_2@C_{98}$ and $Gd_2C_2@C_{104}$, will likely be discovered. Tagmatarchis et al. previously isolated 17 didysprosium metallofullerenes, namely Dy_2C_{80}(I), Dy_2C_{82}(I), Dy_2C_{84}(I, II, III), Dy_2C_{86}(I, II), Dy_2C_{88}(I, II), Dy_2C_{90} (I, II, III), Dy_2C_{92}(I, II, III), and Dy_2C_{94}(I, II) [131], among which only the three Dy_2C_{84} isomers were hitherto proposed to be MCCFs [33,34]. An intriguing question arises: how many Dy-based MCCFs members are hiding among them? In addition to the two Dy_2C_{94} isomers, Yang et al. also prepared and isolated Dy_2C_{98} and Dy_2C_{100} [101]. The latter was suggested as a di-EMF $Dy_2@D_5(285913)$-C_{100} structure in the subsequent theoretical studies [145,172]. No convincing experimental evidence is available so far, however, and one still cannot preclude an alternative formula of a MCCF $Dy_2C_2@C_{98}$.

Partially due to their unfavorable HOMO-LUMO energy gaps, giant fullerenes are generally poorly soluble in common solvents. The largest crystallographically characterized EMF so far is Sm_2C_{104} (I), which is a conventional di-EMF, $Sm_2@D_{3d}$-C_{104} [6,132]. In addition to this isomer, two other isomers Sm_2C_{104} (II, III) with lower production yields remain unidentified. The UV–vis–NIR spectra indicated that their cage geometries are different from the most

abundant isomer (I). Thus, an alternative $Sm_2C_2@C_{102}$ carbide structure likely exists among them.

In sharp contrast to conventional EMFs, no lanthanum-containing MCCF has been experimentally reported. Along with La_2C_{80}, insoluble compositions ranging from La_2C_{74} to La_2C_{100}, and from La_3C_{102} to La_3C_{126}, were detected in mass spectra but were not structurally identified [10]. The recent breakthrough work by Balch and coworkers is significant and encouraging. By using chlorobenzene instead of common toluene as an HPLC eluent, they successfully detected a variety of higher fullerenes ranging from La_2C_{90} to La_2C_{138} and characterized an abundant species as di-EMF $La_2@D_5(285913)$-C_{100} using single-crystal XRD [5]. Therefore, there is a possibility of finding La-based MCCF in these massive samples, especially for those featuring large tubular shapes [173].

In summary, MCCFs are ubiquitous. MCCFs coexist with conventional EMFs or even cover all isomeric forms of a given metallofullerene. The carbon encapsulation stabilizes the otherwise labile metal cluster and leads to brand-new intramolecular interactions. The incorporation dramatically modifies the electronic structure of an MCCF, which consequently exhibits entirely different properties than conventional EMFs of the same cage size. The chemical functionalization endows MCCFs with versatile properties for many practical applications. Despite the difficulties of precise structural identification, with the advance of rapid separation and characterization methods [162,171,174], undoubtedly, many new MCCFs members will continuously appear in the near future, and keep us refreshed.

Acknowledgments

Support in China by NSFC (21103224 and 51172060) and the National Basic Research Program of China (973 Programs, 2011CB612301), and in USA by Department of Defense (Grant W911NF-12-1-0083) and partially by NSF (Grant EPS-1010094) is gratefully acknowledged.

References

[1] H. Shinohara, Rep. Prog. Phys. 63 (2000) 843.
[2] T. Akasaka, S. Nagase, Endofullerenes: A New Family of Carbon Clusters, Kluwer Academic Publishers, Dordrecht, 2002.
[3] For recent reviews, see;
(a) H. Cong, B. Yu, T. Akasaka, X. Lu, Coord. Chem. Rev. 257 (2013) 2880;
(b) A.A. Popov, S. Yang, L. Dunsch, Chem. Rev. 113 (2013) 5989;
(c) X. Lu, L. Feng, T. Akasaka, S. Nagase, Chem. Soc. Rev. 41 (2012) 7723;
(d) A.A. Popov, S.M. Avdoshenko, A.M. Pendás, L. Dunsch, Chem. Commun. 48 (2012) 8031;
(e) M. Rudolf, S. Wolfrum, D.M. Guldi, L. Feng, T. Tsuchiya, T. Akasaka, L. Echegoyen, Chem. Eur. J. 18 (2012) 5136;
(f) S. Yang, F. Liu, C. Chen, M. Jiao, T. Wei, Chem. Commun. 47 (2011) 11822;
(g) X. Lu, T. Akasaka, S. Nagase, Chem. Commun. 47 (2011) 5942;
(h) A. Rodríguez-Fortea, A.L. Balch, J.M. Poblet, Chem. Soc. Rev. 40 (2011) 3551;
(i) S. Osuna, M. Swart, M. Solà, Phys. Chem. Chem. Phys. 13 (2011) 3585.
[4] H.W. Kroto, Nature 329 (1987) 529.
[5] C.M. Beavers, H. Jin, H. Yang, Z. Wang, X. Wang, H. Ge, Z. Liu, B.Q. Mercado, M.M. Olmstead, A.L. Balch, J. Am. Chem. Soc. 133 (2011) 15338.
[6] B.Q. Mercado, A. Jiang, H. Yang, Z. Wang, H. Jin, Z. Liu, M.M. Olmstead, A.L. Balch, Angew. Chem. Int. Ed. 48 (2009) 9114.
[7] J.R. Heath, S.C. O'Brien, Q. Zhang, Y. Liu, R.F. Curl, H.W. Kroto, F.K. Tittel, R.E. Smalley, J. Am. Chem. Soc. 107 (1985) 7779.
[8] H.W. Kroto, J.R. Heath, S.C. O'Brien, R.F. Curl, R.E. Smalley, Nature 318 (1985) 162.
[9] Y. Chai, T. Guo, C.M. Jin, R.E. Haufler, L.P.F. Chibante, J. Fure, L.H. Wang, J.M. Alford, R.E. Smalley, J. Phys. Chem. 95 (1991) 7564.
[10] M.M. Alvarez, E.G. Gillan, K. Holczer, R.B. Kaner, K.S. Min, R.L. Whetten, J. Phys. Chem. 95 (1991) 10561.
[11] S. Stevenson, G. Rice, T. Glass, K. Harich, F. Cromer, M.R. Jordan, J. Craft, E. Hadju, R. Bible, M.M. Olmstead, K. Maitra, A.J. Fisher, A.L. Balch, H.C. Dorn, Nature 401 (1999) 55.
[12] For a very recent review on TNT EMFs, please see J. Zhang, S. Stevenson, H.C. Dorn, Acc. Chem. Res. 46 (2013) 1548.
[13] C.R. Wang, T. Kai, T. Tomiyama, T. Yoshida, Y. Kobayashi, E. Nishibori, M. Takata, M. Sakata, H. Shinohara, Angew. Chem. Int. Ed. 40 (2001) 397.
[14] M. Krause, F. Ziegs, A.A. Popov, L. Dunsch, ChemPhysChem 8 (2007) 537.
[15] T.-S. Wang, L. Feng, J.-Y. Wu, W. Xu, J.-F. Xiang, K. Tan, Y.-H. Ma, J.-P. Zheng, L. Jiang, X. Lu, C.-Y. Shu, C.-R. Wang, J. Am. Chem. Soc. 132 (2010) 16362.
[16] S. Stevenson, M.A. Mackey, M.A. Stuart, J.P. Phillips, M.L. Easterling, C.J. Chancellor, M.M. Olmstead, A.L. Balch, J. Am. Chem. Soc. 130 (2008) 11844.
[17] L. Dunsch, S. Yang, L. Zhang, A. Svitova, S. Oswald, A.A. Popov, J. Am. Chem. Soc. 132 (2010) 5413.
[18] Z.Q. Shi, X. Wu, C.R. Wang, X. Lu, H. Shinohara, Angew. Chem. Int. Ed. 45 (2006) 2107.
[19] D.-L. Chen, W.Q. Tian, J.-K. Feng, C.-C. Sun, ChemPhysChem 9 (2008) 454.
[20] Y. Feng, T. Wang, J. Wu, L. Feng, J. Xiang, Y. Ma, Z. Zhang, L. Jiang, C. Shu, C. Wang, Nanoscale 5 (2013) 6704.
[21] J. Wu, T. Wang, C. Shu, X. Lu, C. Wang, Chin. J. Chem. 30 (2012) 765.
[22] T. Yumura, Y. Sato, K. Suenaga, S. Iijima, J. Phys. Chem. B 109 (2005) 20251.
[23] K. Tan, X. Lu, Chem. Commun. (2005) 4444.
[24] Y. Sato, T. Yumura, K. Suenaga, H. Moribe, D. Nishide, M. Ishida, H. Shinohara, S. Iijima, Phys. Rev. B 73 (2006) 193401.
[25] X. Wu, X. Lu, K. Tan, Q. Zhang, J. Nanosci. Nanotechnol. 7 (2007) 1346.
[26] H. Kurihara, X. Lu, Y. Iiduka, N. Mizorogi, Z. Slanina, T. Tsuchiya, T. Akasaka, S. Nagase, J. Am. Chem. Soc. 133 (2011) 2382.
[27] Y. Iiduka, T. Wakahara, T. Nakahodo, T. Tsuchiya, A. Sakuraba, Y. Maeda, T. Akasaka, K. Yoza, E. Horn, T. Kato, M.T.H. Liu, N. Mizorogi, K. Kobayashi, S. Nagase, J. Am. Chem. Soc. 127 (2005) 12500.
[28] E. Nishibori, I. Terauchi, M. Sakata, M. Takata, Y. Ito, T. Sugai, H. Shinohara, J. Phys. Chem. B 110 (2006) 19215.
[29] T.-S. Wang, N. Chen, J.-F. Xiang, B. Li, J.-Y. Wu, W. Xu, L. Jiang, K. Tan, C.-Y. Shu, X. Lu, C.-R. Wang, J. Am. Chem. Soc. 131 (2009) 16646.
[30] Y. Iiduka, T. Wakahara, K. Nakajima, T. Tsuchiya, T. Nakahodo, Y. Maeda, T. Akasaka, N. Mizorogi, S. Nagase, Chem. Commun. (2006) 2057.
[31] X. Lu, K. Nakajima, Y. Iiduka, H. Nikawa, N. Mizorogi, Z. Slanina, T. Tsuchiya, S. Nagase, T. Akasaka, J. Am. Chem. Soc. 133 (2011) 19553.
[32] X. Lu, K. Nakajima, Y. Iiduka, H. Nikawa, T. Tsuchiya, N. Mizorogi, Z. Slanina, S. Nagase, T. Akasaka, Angew. Chem. Int. Ed. 51 (2012) 5889.
[33] T. Inoue, T. Tomiyama, T. Sugai, H. Shinohara, Chem. Phys. Lett. 382 (2003) 226.
[34] T. Inoue, T. Tomiyama, T. Sugai, T. Okazaki, T. Suematsu, N. Fujii, H. Utsumi, K. Nojima, H. Shinohara, J. Phys. Chem. B 108 (2004) 7573.
[35] H. Okimoto, R. Kitaura, T. Nakamura, Y. Ito, Y. Kitamura, T. Akachi, D. Ogawa, N. Imazu, Y. Kato, Y. Asada, T. Sugai, H. Osawa, M. Matsushita, T. Muro, H. Shinohara, J. Phys. Chem. C 112 (2008) 6103.
[36] Y. Ito, T. Okazaki, S. Okubo, M. Akachi, Y. Ohno, T. Mizutani, T. Nakamura, R. Kitaura, T. Sugai, H. Shinohara, ACS Nano 1 (2007) 456.
[37] J. Zhang, T. Fuhrer, W. Fu, J. Ge, D.W. Bearden, J. Dallas, J. Duchamp, K. Walker, H. Champion, H. Azurmendi, K. Harich, H.C. Dorn, J. Am. Chem. Soc. 134 (2012) 8487.
[38] T. Yang, X. Zhao, S.-T. Li, S. Nagase, Inorg. Chem. 51 (2012) 11223.
[39] J. Zhang, F.L. Bowles, D.W. Bearden, W.K. Ray, T. Fuhrer, Y. Ye, C. Dixon, K. Harich, R.F. Helm, M.M. Olmstead, A.L. Balch, H.C. Dorn, Nat. Chem. 5 (2013) 880.
[40] Y. Nishimoto, Z. Wang, K. Morokuma, S. Irle, Phys. Status Solidi B 249 (2012) 324.
[41] W. Xu, T.-S. Wang, J.-Y. Wu, Y.-H. Ma, J.-P. Zheng, H. Li, B. Wang, L. Jiang, C.-Y. Shu, C.-R. Wang, J. Phys. Chem. C 115 (2011) 402.
[42] B.G. Burke, J. Chan, K.A. Williams, T. Fuhrer, W. Fu, H.C. Dorn, A.A. Puretzky, D.B. Geohegan, Phys. Rev. B 83 (2011) 115457.
[43] B.G. Burke, T.-W. Chan, K.A. Williams, J. Ge, C. Shu, W. Fu, H.C. Dorn, A. Puretzky, D. Geohegan, Mater. Res. Soc. Symp. Proc. 1204 (2010) K10-20.
[44] H. Yang, C. Lu, Z. Liu, H. Jin, Y. Che, M.M. Olmstead, A.L. Balch, J. Am. Chem. Soc. 130 (2008) 17296.
[45] X. Lu, T. Akasaka, S. Nagase, Acc. Chem. Res. 46 (2013) 1627.
[46] H. Shinohara, H. Yamaguchi, N. Hayashi, H. Sato, M. Ohkohchi, Y. Ando, Y. Saito, J. Phys. Chem. 97 (1993) 4259.
[47] C.-R. Wang, M. Inakuma, H. Shinohara, Chem. Phys. Lett. 300 (1999) 379.
[48] P.W. Fowler, D.E. Manolopoulos, An Atlas of Fullerenes, Clarendon, Oxford, 1995.
[49] In this work, each structure is labeled with parent cage symmetry, followed by Fowler spiral numbering from Ref. [48] in parenthesis.
[50] Y. Yamazaki, K. Nakajima, T. Wakahara, T. Tsuchiya, M.O. Ishitsuka, Y. Maeda, T. Akasaka, M. Waelchli, N. Mizorogi, S. Nagase, Angew. Chem. Int. Ed. 47 (2008) 7905.
[51] S. Taubert, M. Straka, T.O. Pennanen, D. Sundholm, J. Vaara, Phys. Chem. Chem. Phys. 10 (2008) 7158.
[52] M. Takata, B. Umeda, E. Nishibori, M. Sakata, Y. Saito, M. Ohno, H. Shinohara, Nature 377 (1995) 46.
[53] M. Krause, M. Hulman, H. Kuzmany, O. Dubay, G. Kresse, K. Vietze, G. Seifert, C. Wang, H. Shinohara, Phys. Rev. Lett. 93 (2004) 137403.
[54] H. Wu, K. Deng, G. Lu, Y. Yuan, J. Yang, X. Wang, J. Phys. Condens. Matter. 18 (2006) 7115.
[55] H. Kurihara, X. Lu, Y. Iiduka, H. Nikawa, M. Hachiya, N. Mizorogi, Z. Slanina, T. Tsuchiya, S. Nagase, T. Akasaka, Inorg. Chem. 51 (2012) 746.
[56] C.-R. Wang, T.J.S. Dennis, T. Itho, T. Ogawa, H. Shinohara, Electrochem. Soc. Proc. 99–12 (1999) 795.
[57] H. Zheng, X. Zhao, W.-W. Wang, T. Yang, S. Nagase, J. Chem. Phys. 137 (2012) 014308.
[58] S. Stevenson, H.C. Dorn, P. Burbank, K. Harich, J. Haynes, C.H. Kiang, J.R. Salem, M.S. de Vries, P.H.M. van Loosdrecht, R.D. Johnson, C.S. Yannoni, D.S. Bethune, Anal. Chem. 66 (1994) 2675.

[59] S. Nagase, K. Kobayashi, Chem. Phys. Lett. 276 (1997) 55.
[60] S. Nagase, K. Kobayashi, T. Akasaka, J. Mol. Struc. (THEOCHEM) 461–462 (1999) 97.
[61] J. Laskin, T. Peres, A. Khong, H.A. Jiménez-Vázquez, R.J. Cross, M. Saunders, D.S. Bethune, M.S. de Vries, C. Lifshitz, Int. J. Mass Spectrom. 185/186/187 (1999) 61.
[62] D. Liu, F. Hagelberg, Int. J. Quant. Chem. 107 (2007) 2253.
[63] E. Krokos, J. Phys. Chem. C 114 (2010) 7626.
[64] C.R. Wang, L. Gan, C. Bai, H. Shinohara, Chin. Particuol. 2 (2004) 189.
[65] Z. Xu, T. Nakane, H. Shinohara, J. Am. Chem. Soc. 118 (1996) 11309.
[66] T. Sugai, M. Inakuma, R. Hudgins, P. Dugourd, J.L. Fye, M.F. Jarrold, H. Shinohara, J. Am. Chem. Soc. 123 (2001) 6427.
[67] B. Cao, M. Hasegawa, K. Okada, T. Tomiyama, T. Okazaki, K. Suenaga, H. Shinohara, J. Am. Chem. Soc. 123 (2001) 9679.
[68] K. Iwasaki, S. Hino, D. Yoshimura, B. Cao, T. Okazaki, H. Shinohara, Chem. Phys. Lett. 397 (2004) 169.
[69] R. Jaffiol, A. Débarre, C. Julien, D. Nutarelli, P. Tchénio, A. Taninaka, B. Cao, T. Okazaki, H. Shinohara, Phys. Rev. B 68 (2003) 014105.
[70] S. Hino, K. Iwasaki, N. Wanita, D. Yoshimura, B. Cao, T. Okazaki, H. Shinohara, Full Nanotubes Carbon Nanostruct. 12 (2004) 33.
[71] A. Débarre, R. Jaffiol, C. Julien, A. Richard, D. Nutarelli, P. Tchénio, Chem. Phys. Lett. 380 (2003) 6.
[72] A.N. Enyashin, Yu.N. Makurin, A.L. Ivanovskii, Comp. Mater. Sci. 36 (2006) 26.
[73] A.A. Popov, L. Dunsch, J. Am. Chem. Soc. 130 (2008) 17726.
[74] S. Hino, M. Kato, D. Yoshimura, H. Moribe, H. Umemoto, Y. Ito, T. Sugai, H. Shinohara, M. Otani, Y. Yoshimoto, S. Okada, Phys. Rev. B 75 (2007) 125418.
[75] K. Akiyama, K. Sueki, T. Kodama, K. Kikuchi, Y. Takigawa, H. Nakahara, I. Ikemoto, M. Katada, Chem. Phys. Lett. 317 (2000) 490.
[76] H. Shinohara, H. Sato, M. Ohkohchi, Y. Ando, T. Kodama, T. Shida, T. Kato, Y. Saito, Nature 357 (1992) 52.
[77] H. Kurihara, X. Lu, Y. Iiduka, H. Nikawa, N. Mizorogi, Z. Slanina, T. Tsuchiya, S. Nagase, T. Akasaka, J. Am. Chem. Soc. 134 (2012) 3139.
[78] H. Kurihara, X. Lu, Y. Iiduka, N. Mizorogi, Z. Slanina, T. Tsuchiya, S. Nagase, T. Akasaka, Chem. Commun. 48 (2012) 1290.
[79] C.S. Yannoni, M. Hoinkis, M.S. de Vries, D.S. Bethune, J.R. Salem, M.S. Crowder, R.D. Johnson, Science 256 (1992) 1191.
[80] L.B. Knight, R.W. Woodward, R.J. Van Zee, W. Weltner Jr., J. Chem. Phys. 79 (1983) 5820.
[81] H. Shinohara, H. Yamaguchi, N. Hayashi, H. Sato, M. Inagaki, Y. Saito, S. Bandow, H. Kitagawa, T. Mitani, H. Inokuchi, Mater. Sci. Eng. B 19 (1993) 25.
[82] H. Shinohara, M. Inakuma, N. Hayashi, H. Sato, Y. Saito, T. Kato, S. Bandow, J. Phys. Chem. 98 (1994) 8597.
[83] P.H.M. van Loosdrecht, R.D. Johnson, M.S. de Vries, C.-H. Kiang, D.S. Bethune, H.C. Dorn, P. Burbank, S. Stevenson, Phys. Rev. Lett. 73 (1994) 3415.
[84] S. Suzuki, Y. Kojima, Y. Nakao, T. Wakabayashi, S. Kawata, K. Kikuchi, Y. Achiba, T. Kato, Chem. Phys. Lett. 229 (1994) 512.
[85] T. Kato, S. Bandou, M. Inakuma, H. Shinohara, J. Phys. Chem. 99 (1995) 856.
[86] A. Bartl, L. Dunsch, Synth. Met. 121 (2001) 1147.
[87] T. Kato, S. Okubo, M. Inakuma, H. Shinohara, Phys. Solid State 44 (2002) 410.
[88] J. Rahmer, L. Dunsch, H. Dorn, J. Mende, M. Mehring, Magn. Reson. Chem. 43 (2005) S192.
[89] M.R. Anderson, H.C. Dorn, S. Stevenson, P.M. Burbank, J.R. Gibson, J. Am. Chem. Soc. 119 (1997) 437.
[90] T. Wakahara, A. Sakuraba, Y. Iiduka, M. Okamura, T. Tsuchiya, Y. Maeda, T. Akasaka, S. Okubo, T. Kato, K. Kobayashi, S. Nagase, K.M. Kadish, Chem. Phys. Lett. 398 (2004) 553.
[91] M. Takata, E. Nishibori, M. Sakata, M. Inakuma, E. Yamamoto, H. Shinohara, Phys. Rev. Lett. 83 (1999) 2214.
[92] J.R. Ungerer, T. Hughbanks, J. Am. Chem. Soc. 115 (1993) 2054.
[93] K. Kobayashi, S. Nagase, Chem. Phys. Lett. 313 (1999) 45.
[94] D.M.P. Mingos, T. Slee, Z. Lin, Chem. Rev. 90 (1990) 383.
[95] X. Lu, Z. Chen, Chem. Rev. 105 (2005) 3643.
[96] K. Tan, X. Lu, J. Phys. Chem. A 110 (2006) 1171.
[97] A.A. Popov, L. Zhang, L. Dunsch, ACS Nano 4 (2010) 795.
[98] W. Xu, L. Feng, M. Calvaresi, J. Liu, Y. Liu, B. Niu, Z. Shi, Y. Lian, F. Zerbetto, J. Am. Chem. Soc. 135 (2013) 4187.
[99] N. Tagmatarchis, E. Aslanis, K. Prassides, H. Shinohara, Chem. Mater. 13 (2001) 2374.
[100] Y. Lian, Z. Shi, X. Zhou, Z. Gu, Chem. Mater. 16 (2004) 1704.
[101] S. Yang, L. Dunsch, Angew. Chem. Int. Ed. 45 (2006) 1299.
[102] B.G. Burke, J. Chan, K.A. Williams, J. Ge, C. Shu, W. Fu, H.C. Dorn, J.G. Kushmerick, A.A. Puretzky, D.B. Geohegan, Phys. Rev. B 81 (2010) 115423.
[103] J.-Y. Wu, W. Xu, T.-S. Wang, L. Jiang, C.-Y. Shu, C.-R. Wang, J. Nanosci. Nanotechnol. 12 (2012) 2254.
[104] K. Tan, X. Lu, C.R. Wang, J. Phys. Chem. B 110 (2006) 11098.
[105] C.B. Kah, J. Nathaniel, K. Suggs, X.-Q. Wang, J. Phys. Chem. C 114 (2010) 13017.
[106] Z. Chen, C.B. Kah, X.-Q. Wang, Chem. Phys. Lett. 506 (2011) 230.
[107] Q.L. Lu, W.J. Song, J.W. Meng, J.G. Wan, J. Mol. Model. 19 (2013) 1205.
[108] E. Yamamoto, M. Tansho, T. Tomiyama, H. Shinohara, H. Kawahara, Y. Kobayashi, J. Am. Chem. Soc. 118 (1996) 2293.
[109] M. Inakuma, E. Yamamoto, T. Kai, C.-R. Wang, T. Tomiyama, H. Shinohara, T.J.S. Dennis, M. Hulman, M. Krause, H. Kuzmany, J. Phys. Chem. B 104 (2000) 5072.
[110] X.-D. Wang, Q.K. Xue, T. Hashizume, H. Shinohara, Y. Nishina, T. Sakurai, Phys. Rev. B 48 (1993) 15492.
[111] H. Shinohara, N. Hayashi, H. Sato, Y. Saito, X.-D. Wang, T. Hashizume, T. Sakurai, J. Phys. Chem. 97 (1993) 13438.
[112] R. Beyers, C.-H. Kiang, R.D. Johnson, J.R. Salem, M.S. de Vries, C.S. Yannoni, D.S. Bethune, H.C. Dorn, P. Burbank, K. Harich, S. Stevenson, Nature 370 (1994) 196.
[113] T. Takahashi, A. Ito, M. Inakuma, H. Shinohara, Phys. Rev. B 52 (1995) 13812.
[114] Y. Miyake, S. Suzuki, Y. Kojima, K. Kikuchi, K. Kobayashi, S. Nagase, M. Kainosho, Y. Achiba, Y. Maniwa, K. Fisher, J. Phys. Chem. 100 (1996) 9579.
[115] M. Hulman, T. Pichler, H. Kuzmany, F. Zerbetto, E. Yamamoto, H.N. Shinohara, J. Mol. Struct. 408/409 (1997) 359.
[116] M. Krause, M. Hulman, H. Kuzmany, T.J.S. Dennis, M. Inakuma, H. Shinohara, J. Chem. Phys. 111 (1999) 7976.
[117] M. Krause, M. Hulman, H. Kuzmany, P. Kuran, L. Dunsch, T.J.S. Dennis, M. Inakuma, H. Shinohara, J. Mol. Struct. 521 (2000) 325.
[118] M. Krause, V.N. Popov, M. Inakuma, N. Tagmatarchis, H. Shinohara, P. Georgi, L. Dunsch, H. Kuzmany, J. Chem. Phys. 120 (2004) 1873.
[119] S. Nagase, K. Kobayashi, Chem. Phys. Lett. 231 (1994) 319.
[120] K. Kobayashi, S. Nagase, T. Akasaka, Chem. Phys. Lett. 261 (1996) 502.
[121] M. Takata, E. Nishibori, B. Umeda, M. Sakata, E. Yamamoto, H. Shinohara, Phys. Rev. Lett. 78 (1997) 3330.
[122] K. Suenaga, T. Okazaki, C.-R. Wang, S. Bandow, H. Shinohara, S. Iijima, Phys. Rev. Lett. 90 (2003) 055506.
[123] E. Nishibori, M. Ishihara, M. Takata, M. Sakata, Y. Ito, T. Inoue, H. Shinohara, Chem. Phys. Lett. 433 (2006) 120.
[124] Y. Iiduka, T. Wakahara, K. Nakajima, T. Nakahodo, T. Tsuchiya, Y. Maeda, T. Akasaka, K. Yoza, M.T.H. Liu, N. Mizorogi, S. Nagase, Angew. Chem. Int. Ed. 46 (2007) 5562.
[125] R. Valencia, A. Rodríguez-Fortea, J.M. Poblet, J. Phys. Chem. A 112 (2008) 4550.
[126] S. Hino, N. Wanita, K. Iwasaki, D. Yoshimura, T. Akachi, T. Inoue, Y. Ito, T. Sugai, H. Shinohara, Phys. Rev. B 72 (2005) 195424.
[127] E. Nishibori, S. Narioka, M. Takata, M. Sakata, T. Inoue, H. Shinohara, ChemPhysChem 7 (2006) 345.
[128] A.N. Enyashin, A.L. Ivanovskii, Theor. Exp. Chem. 40 (2004) 273.
[129] W. Fu, L. Xu, H. Azurmendi, J. Ge, T. Fuhrer, T. Zuo, J. Reid, C. Shu, K. Harich, H.C. Dorn, J. Am. Chem. Soc. 131 (2009) 11762.
[130] N. Tagmatarchis, E. Aslanis, H. Shinohara, K. Prassides, J. Phys. Chem. B 104 (2000) 11010.
[131] N. Tagmatarchis, H. Shinohara, Chem. Mater. 12 (2000) 3222.
[132] H. Yang, H. Jin, B. Hong, Z. Liu, C.M. Beavers, H. Zhen, Z. Wang, B.Q. Mercado, M.M. Olmstead, A.L. Balch, J. Am. Chem. Soc. 133 (2011) 16911.
[133] P. Jin, Z. Zhou, C. Hao, Z. Gao, K. Tan, X. Lu, Z. Chen, Phys. Chem. Chem. Phys. 12 (2010) 12442.
[134] Y. Feng, T. Wang, J. Wu, Y. Ma, Z. Zhang, L. Jiang, C. Ge, C. Shu, C. Wang, Chem. Commun. 49 (2013) 2148.
[135] J. Wu, T. Wang, Y. Ma, L. Jiang, C. Shu, C. Wang, J. Phys. Chem. C 115 (2011) 23755.
[136] Y. Gao, F. Zhang, Q. Meng, X. Sun, D. Wang, Comput. Theor. Chem. 1014 (2013) 56.
[137] D.-L. Wang, H.-L. Xu, Z.-M. Su, G. Xin, Phys. Chem. Chem. Phys. 14 (2012) 15099.
[138] K. Komatsu, M. Murata, Y. Murata, Science 307 (2005) 238.
[139] S. Yang, C. Chen, F. Liu, Y. Xie, F. Li, M. Jiao, M. Suzuki, T. Wei, S. Wang, Z. Chen, X. Lu, T. Akasaka, Sci. Rep. 3 (2013) 1487.
[140] S. Roszak, K. Balasubramanian, J. Phys. Chem. A 102 (1998) 6004.
[141] J.A. Dean, Lange's Handbook of Chemistry, 15th ed., McGram-Hill Inc., 1999.
[142] Y. Ma, T. Wang, J. Wu, Y. Feng, H. Li, L. Jiang, C. Shu, C. Wang, J. Phys. Chem. Lett. 4 (2013) 464.
[143] M. Garcia-Borràs, S. Osuna, J.M. Luis, M. Swart, M. Solà, Chem. Eur. J. 18 (2012) 7141.
[144] J.M. Campanera, C. Bo, J.M. Poblet, Angew. Chem. Int. Ed. 44 (2005) 7230.
[145] R. Valencia, A. Rodríguez-Fortea, J.M. Poblet, Chem. Commun. (2007) 4161.
[146] A.A. Popov, L. Dunsch, J. Am. Chem. Soc. 129 (2007) 11835.
[147] A. Rodríguez-Fortea, N. Alegret, A.L. Balch, J.M. Poblet, Nat. Chem. 2 (2010) 955.
[148] A.A. Popov, L. Dunsch, Chem. Eur. J. 15 (2009) 9707.
[149] R. Sumathi, M. Hendrickx, J. Phys. Chem. A 103 (1999) 585.
[150] P.W. Dunk, N.K. Kaiser, C.L. Hendrickson, J.P. Quinn, C.P. Ewels, Y. Nakanishi, Y. Sasaki, H. Shinohara, A.G. Marshall, H.W. Kroto, Nat. Commun. 3 (2012) 855.
[151] T. Miyazaki, R. Sumii, H. Umemoto, H. Okimoto, Y. Ito, T. Sugai, H. Shinohara, T. Zaima, H. Yagi, S. Hino, Chem. Phys. 397 (2012) 87.
[152] T. Akasaka, S. Nagase, K. Kobayashi, M. Wälchli, K. Yamamoto, H. Funasaka, M. Kako, T. Hoshino, T. Erata, Angew. Chem. Int. Ed. 36 (1997) 1643.
[153] K.H. Michel, B. Verberck, M. Hulman, H. Kuzmany, M. Krause, J. Chem. Phys. 126 (2007) 064304.
[154] T. Wakahara, M. Yamada, S. Takahashi, T. Nakahodo, T. Tsuchiya, Y. Maeda, T. Akasaka, M. Kako, K. Yoza, E. Horn, N. Mizorogi, S. Nagase, Chem. Commun. (2007) 2680.
[155] M. Yamada, T. Nakahodo, T. Wakahara, T. Tsuchiya, Y. Maeda, T. Akasaka, M. Kako, K. Yoza, E. Horn, N. Mizorogi, K. Kobayashi, S. Nagase, J. Am. Chem. Soc. 127 (2005) 14570.
[156] T. Kato, J. Mol. Struct. 838 (2007) 84.
[157] T. Wang, J. Wu, W. Xu, J. Xiang, X. Lu, B. Li, L. Jiang, C. Shu, C. Wang, Angew. Chem. Int. Ed. 49 (2010) 1786.
[158] M. Garcia-Borràs, S. Osuna, J.M. Luis, M. Swart, M. Solà, Chem. Eur. J. 19 (2013) 14931.
[159] T. Wang, J. Wu, Y. Feng, Y. Ma, L. Jiang, C. Shu, C. Wang, Dalton Trans. 41 (2012) 2567.

[160] H. Kurihara, Y. Iiduka, Y. Rubin, M. Waelchli, N. Mizorogi, Z. Slanina, T. Tsuchiya, S. Nagase, T. Akasaka, J. Am. Chem. Soc. 134 (2012) 4092.
[161] C.-H. Chen, W.-Y. Yeh, Y.-H. Liu, G.-H. Lee, Angew. Chem. Int. Ed. 51 (2012) 13046.
[162] K. Akiyama, T. Hamano, Y. Nakanishi, E. Takeuchi, S. Noda, Z. Wang, S. Kubuki, H. Shinohara, J. Am. Chem. Soc. 134 (2012) 9762.
[163] Z. Wang, Y. Nakanishi, S. Noda, K. Akiyama, H. Shinohara, J. Phys. Chem. C 116 (2012) 25563.
[164] S. Sato, S. Seki, G. Luo, M. Suzuki, J. Lu, S. Nagase, T. Akasaka, J. Am. Chem. Soc. 134 (2012) 11681.
[165] M. Mikawa, H. Kato, M. Okumura, M. Narazaki, Y. Kanazawa, N. Miwa, H. Shinohara, Bioconjugate Chem. 12 (2001) 510.
[166] E.B. Iezzi, J.C. Duchamp, K.R. Fletcher, T.E. Glass, H.C. Dorn, Nano Lett. 2 (2002) 1187.
[167] J.H. Warner, Y. Ito, M. Zaka, L. Ge, T. Akachi, H. Okimoto, K. Porfyrakis, A.A.R. Watt, H. Shinohara, G.A.D. Briggs, Nano Lett. 8 (2008) 2328.
[168] Y. Iijima, K. Ohashi, N. Imazu, R. Kitaura, K. Kanazawa, A. Taninaka, O. Takeuchi, H. Shigekawa, H. Shinohara, J. Phys. Chem. C 117 (2013) 6966.
[169] S. Maki, E. Nishibori, Y. Kitamura, R. Kitaura, M. Ishihara, T. Aono, S. Aoyagi, M. Takata, M. Sakata, H. Shinohara, Cryst. Growth Des. 13 (2013) 3632.
[170] B. Cao, K. Suenaga, T. Okazaki, H. Shinohara, J. Phys. Chem. B 106 (2002) 9295.
[171] S. Maki, E. Nishibori, I. Terauchi, M. Ishihara, S. Aoyagi, M. Sakata, M. Taktata, H. Umemoto, T. Inoue, H. Shinohara, J. Am. Chem. Soc. 135 (2013) 918.
[172] T. Yang, X. Zhao, S. Nagase, Phys. Chem. Chem. Phys. 13 (2011) 5034.
[173] X. Lu, T. Akasaka, S. Nagase, Angew. Chem. Int. Ed. 51 (2012) 2812.
[174] S. Stevenson, K.A. Rottinger, Inorg. Chem. 52 (2013) 9606.